Universidade Federal do Rio Grande do Sul
Instituto de Fisica
Departamento de Astronomia

A Chromodynamical Analysis of S0 Galaxies with Globular Clusters and Planetary Nebulae

Emilio J. B. Zanatta

Msc. dissertation under the supervision of Prof. Dr. Ana Leonor Chies Santiago Santos and colaboration of Dr. Arianna Cortesi submitted to *Instituto de Física – Universidade Federal do Rio Grande do Sul* (UFRGS) as part of the fulfilment to obtain the master's degree in physics.

Porto Alegre, July 2017

Acknowledgements

To my mother, who raised me to always be honest above everything; to my father that showed me how learning was fun and to my grandmother who helped me reach whatever heights I dreamed of. To Maitê and Luisa, that always believed in me and recognised my work even when everyone else did not. Also, obviously to Sofia and Odin for receiving me at home every single day with joy, even when I failed miserably elsewhere.

Thanks also to the colleagues and professors I've met in these two years at UFRGS, for the ocassional help that kept me from being stuck. To my supervisors Ana and Arianna, who tried to teach me everything they knew whenever they were available. I would also like to thank my professors and friends at UFJF, from whom I learned to love physics.

Finally, a big thanks to methylphenidate.

'It is almost irresistible for humans to believe that we have some special relation to the universe (...) It is very hard to realise that this is all just a tiny part of an overwhelmingly hostile universe. It is even harder to realise that this present universe has evolved from an unspeakably unfamiliar early condition, and faces a future extinction of endless cold or intolerable heat. The more the universe seems comprehensible, the more it also seems pointless. But if there is no solace in the fruits of our research, there is at least some consolation in the research itself. (...) The effort to understand the universe is one of the very few things that lifts human life a little above the level of farce, and gives it some of the grace of tragedy.'

Steven Weinberg, 1993, in the epilogue of The First Three Minutes

Abstract

Lenticular galaxies are proposed to be a transition phase between *early-type* and *late-type* galaxies, as they share properties that can be found in either one or the other type. Therefore, the study of the evolution of such galaxy morphology can shed light on the understating of galaxy evolution in a global way. In this work we study the kinematics of the globular cluster (GC) systems of three lenticular galaxies: NGC 2768, NGC 3115 and NGC 7457, using previously obtained kinematics from planetary nebulae (PNe). Globular clusters are ubiquitously found in luminous galaxies and can be used as tracers of their host galaxies' assembly histories through its kinematics and stellar population parameters. PNe, on the other hand, can be used as discrete kinematic tracers of the overall stellar population of their parent galaxies. *The broad goal of this dissertation is to infer evidences on the processes that may have contributed to the formation and evolution of such galaxies.* ***Specifically, our main objective is to recover the kinematics of the GCs in their respective components (spheroid and disk) with the derived galaxy kinematics (previously obtained with PNe).*** The present work employs the method developed in Cortesi et al. (2016) to study the GC system of the lenticular galaxy NGC 1023. Here we extend the analysis to three more galaxies and use PNe and GC data from the PN.S (Douglas et al., 2002; Cortesi et al., 2011) and the SLUGGS Survey (Pota et al., 2013; Brodie et al., 2014). The method consists in decomposing the light of a given galaxy in its spheroid and disc components. With such decomposition, we assign probabilities for GCs to belong to the host galaxy disk or spheroid. Furthermore, a maximum likelihood estimation (MLE) is applied to obtain the best fit estimators for the parameters of a gaussian model for the velocity distribution of such tracers. Comparing the results obtained for GCs with the ones previously found for PNe in Cortesi et al. (2011, 2013b), we recalculate the probabilities for each GC to belong to each of the galaxy's components. Associating kinematics to the probabilities previously obtained from photometry, we drastically reduce the impact from observational biases. We show that all galaxies have GCs that can be found in the spheroid and disc components and the ratio between ordered and random motions in those systems is lower than the ones found in regular spiral galaxies. Overall we find that there is great variety in the kinematics of the GC systems in each galaxy, showcasing that the formation and evolutionary processes of these galaxies are also varied. In general, our results point towards a scenario where the assembly of our sample galaxies involved unequal mergers, as suggested in the literature (Bekki et al., 2005; Bournaud et al., 2005).

Resumo

Galáxias lenticulares são consideradas como uma fase de transição entre galáxias *early-type* e *late-type*, uma vez que apresentam características comuns a tanto um quanto ao outro tipo. Devido a isto, o estudo da evolução deste tipo morfológico de galáxia contribui para o entendimento da evolução de galáxias de forma global. Neste trabalho, estudamos a cinemática dos sistemas de aglomerados globulares (GCs) de três galáxias lenticulares: NGC 2768, NGC 3115 e NGC 7457, usando a cinemática obtida previamente de nebulosas planetárias (PNe). Aglomerados globulares são encontrados universalmente em galáxias luminosas e podem ser usados como traçadores dos seus históricos de formação, através de sua cinemática e paramêtros de populações estelares. PNe, por sua vez, podem ser usadas como traçadores discretos da cinemática da população estelar global de suas galáxias hospedeiras. *O objetivo geral desta dissertação é inferir evidências dos processos que contribuíram para a formação e evolução destas galáxias.* ***Especificamente, nosso principal objetivo é obter a cinemática dos GCs em seus respectivos componentes (disco e esferóide) através da cinemática inferida para as galáxias (obtidas previamente com PNe).*** O presente trabalho aplica o método desenvolvido em Cortesi et al. (2016) para estudar o sistema de GCs da galáxia lenticular NGC 1023. Aqui nós estendemos esta análise para mais três galáxias e usamos dados de PNe e GCs do PN.S (Douglas et al., 2002; Cortesi et al., 2016) e do survey SLUGGS (Pota et al., 2013; Brodie et al., 2014). O método consiste em decompor a luz de uma dada galáxia em seus componentes, esferóide e disco. Com esta decomposição, atribuímos probabilidades para os GCs pertencerem ao disco e esferóide da galáxia hospedeira. Posteriormente, uma estimação por máxima verossimilhança (MLE) é aplicada para obtermos os estimadores mais verossímeis para um modelo gaussiano da distribuição de velocidade destes traçadores. Comparando os resultados obtidos para GCs com os previamente encontrados para PNe, em Cortesi et al. (2011, 2013b), recalculamos as probabilidades de cada GC pertencer a cada um dos componentes da galáxia. Associando cinemática às probabilidades previamente obtidas por fotometria, drasticamente reduzimos o impacto de viéses observacionais. Mostramos que todas as galáxias possuem GCs que podem ser encontrados no esferóide e no disco e a razão entre o movimento ordenado e aleatório nestes sistemas é menor do que os encontrados em galáxias espirais regulares. De maneira geral, encontramos grande variedade na cinemática dos sistemas de GCs para cada galáxia, demonstrando que a formação e o processo de evolução destas galáxias é também variado. No todo, nossos resultados indicam um cenário onde a formação das galáxias em nossa

amostra envolveu fusões de galáxias de proporções desiguais, como sugerido na literatura (Bekki et al., 2005; Bournaud et al., 2005).

Notation

The following abbreviations, acronyms and units are used throughout this dissertation:

GCs - Globular Clusters

PNe - Planetary Nebulae

PN.S - Planetary Nebulae Spectrograph (Douglas et al., 2002)

SLUGGS - The SAGES Legacy Unifying Globular and Galaxies Survey (Brodie et al., 2014)

pc - parsecs

kpc - 10^3 pc

Mpc - 10^6 pc

Myr - 10^6 years

Gyr - 10^9 years

C11 - Cortesi et al. (2011)

C13a - Cortesi et al. (2013a)

C13b - Cortesi et al. (2013b)

C16 - Cortesi et al. (2016)

.

Contents

List of Tables

List of Figures

Chapter 1

Introduction

1.1 S0 Galaxies in the Context of Galaxy Evolution

This work intends to unravel clues to the origins and evolutionary histories of lenticular (S0) galaxies by analysing the kinematics of globular clusters (GCs) and planetary nebulae (PNe). In this chapter, we aim to provide a brief historical background on the subject of S0 galaxies within the context of the evolution of different morphological types and the evolution of the Universe itself. Moreover, we will discuss the motivation to study the kinematics of the globular cluster and planetary nebulae systems of lenticular galaxies.

1.1.1 Historical Background

When the objects we know today as galaxies were first observed, what distinguished them from regular objects in the sky was their resolved structure. Nearby galaxies, such as the Andromeda Galaxy (M31) and the Magellanic Clouds, were already described and studied as their own class of objects as early as the 10th century by the Persian astronomer Al-Sufi (Conselice, 2014). As technology progressed, more and more objects known today to be galaxies were catalogued, most notably in the Messier catalogue, first published in 1781 and in the New General Catalogue (NGC), first published in 1888 by John Dreyer based on observations performed mostly by

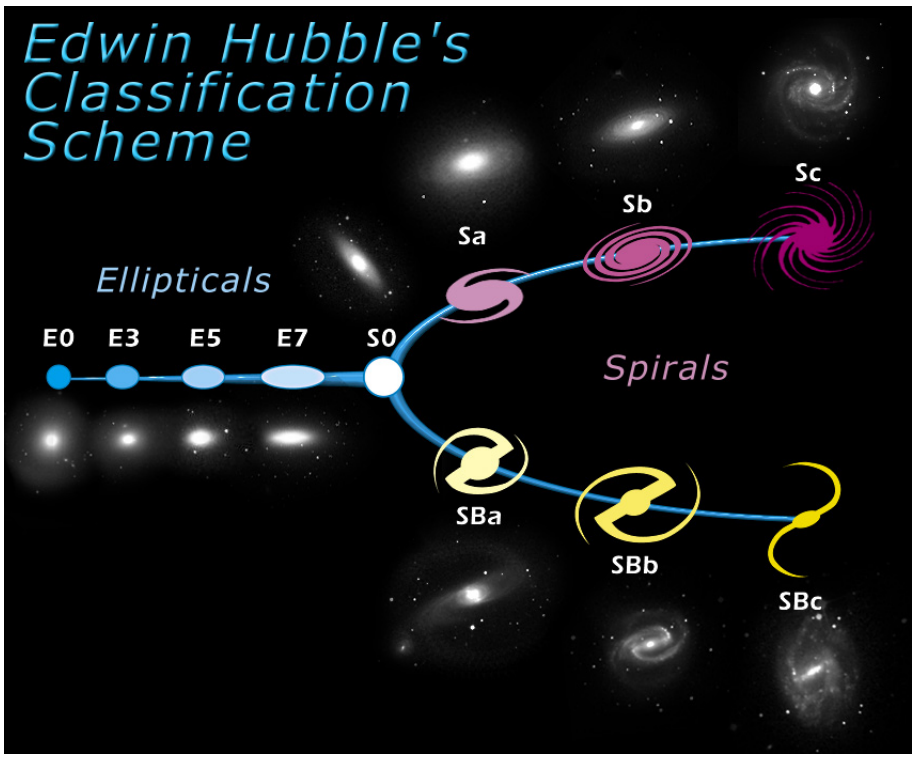

Figure 1.1: Hubble's tuning fork diagram for galaxy classification. Credits: `http://skyserver.sdss.org/dr1/en/proj/advanced/galaxies/images/TuningFork.jpg`.

William and John Herschel.

Until the early 20th century, however, the study of galaxies was restrictively descriptive. With the advent of photography, astronomers were able for the first time to properly study the different morphologies and structures present in external galaxies. Observations performed by Edwin Hubble, in the early 1920s, confirmed that galaxies were indeed external structures and not part of the Milky Way. He also proposed, in 1926, the famous "tuning fork" diagram to classify galaxies based on apparent morphology which hinted at a connection between morphology and galaxy evolution. In his diagram, shown in fig. 1.1, Hubble divided galaxies into two main classes: *early-type* galaxies, comprising elliptical and lenticular galaxies and *late-type* galaxies, comprising spiral galaxies. The latter was divided into two subgroups based on how developed the galaxy's spiral arms structure were and how large its bulge was relative to the disc. In this context, lenticular (S0) galaxies were suggested to be some sort of transition morphology between *early-type* and *late-type* galaxies. This was due to their appearance of a disc, similarly to *late-types*, but lacking spiral structures or gas, displaying prominent bulges and overall redder colours, similarly to elliptical galaxies.

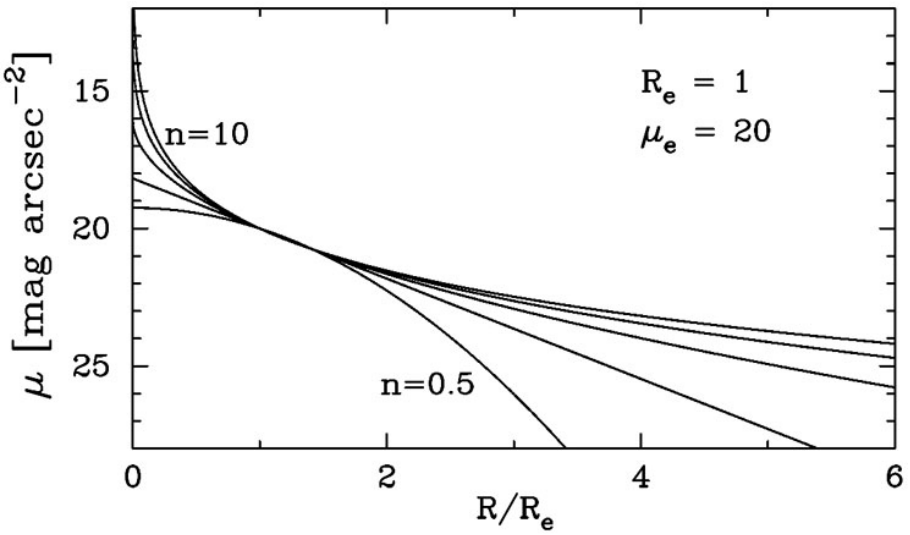

Figure 1.2: Sérsic profiles of surface brightness (eq 1.1) for different values of sérsic index n, adapted from Graham and Driver (2005) and obtained from `https://ned.ipac.caltech.edu/level5/Sept13/Graham/Graham1.html`.

Along the past century, the study of the physics behind the variety of galaxy morphologies improved dramatically as technology progressed, most notably by the advent of Charged Coupled Devices (CCD), that enabled the detailed study of the light distributions in galaxies. In the 1950s and 1960s, astronomers such as Gerard De Vaucouleurs and José Luis Sérsic studied the surface brightness profiles of galaxies and paved the way to the study of their different components and substructures. The Sérsic profile, eq. 1.1 (Sérsic, 1963), describes the general form of the light distribution of galaxies, and has the following form:

$$\mu(R) = \mu_e + \frac{-2.5 b_n}{ln(10)} \Big[\Big(\frac{R}{R_e} \Big)^{1/n} - 1 \Big], \tag{1.1}$$

where μ_e is the intensity at the effective radius R_e, defined as the radius of the circle enclosing half of the total galaxy luminosity, $b_n \approx 2n - 0.237$ (Capaccioli and Caon, 1989) is a parameter directly dependent on the index n, called the *sérsic index*, that is related to the concentration of the galaxy light in the inner regions when compared to its outskirts (see fig. 1.2). Galactic discs can be well described by exponential profiles, which correspond to eq. 1.1 with $n = 1$ (Graham and Driver, 2005), while bulges and spheroidal components of galaxies are better described by values of $n = 4$, when the Sérsic profile turns into the de Vaucouleurs profile (de Vaucouleurs, 1953). Other values for the index n can describe the light of other structures

possibly present in galaxies. Moreover, the combination of Sérsic profiles with different values for n are able to describe the overall light profiles of galaxies effectively enabling one to model a given galaxy by its individual components. Later works developed galaxy light bulge-disc decomposition techniques (Kormendy, 1979) and provide explanations for bars, lenses, rings and other structures observed in galaxies (Combes and Sanders, 1981).

Over the past 20 years, large scale surveys such as the Sloan Digital Sky Survey (SDSS) (York et al., 2000), the Two Micron All-Sky Survey (2MASS) (Skrutskie et al., 2006) and the observations of the Hubble Space Telescope (HST) enabled the discovery of hundreds of thousands of galaxies at many redshifts and an unprecedented amount of data to be studied and analysed. Observations up to redshift $z = 8$ have shown that the structure of galaxies in the early universe were significantly different from what we see today. The star formation rates of galaxies in the early universe were different, as well as their mass, brightness and overall morphologies (Carrasco et al., 2010; Conselice, 2014). This motivated the development of sophisticated statistical approaches to deal with this large amount of data and numerical simulations to model the evolution of galaxies at larger scales and redshifts. In this modern context of galaxy evolution, simulations and observations have shown that S0 galaxies still are a possible transition phase between *early* and *late-type* galaxies, but also stand as interesting science cases by themselves (Oser et al., 2010; Brodie and Strader, 2006).

1.1.2 The Role of S0 Galaxies in Galaxy Evolution

Lenticular galaxies (S0) have clearly defined disc structures alongside prominent bulges. Kinematically, their system is colder than the one of ellipticals, with a rotational velocity associated with the disc and a significant value of velocity dispersion associated with the bulge and the halo surrounding the galaxy. Their location in the Hubble sequence suggests a connection between their formation and the evolution of *early-type* and *late-type* galaxies. However, the formation paths these galaxies have undergone is an open field in current astrophysics with several possibilities proposed along the past decades (Gunn and Gott, 1972; Quilis et al., 2000; Bournaud et al., 2005).

Throughout the 20th century, as technology enabled more distant galaxies to be studied, evidences of the connection between morphology and environment also started to appear and the role of S0 galaxies as tools to understand the evolution of galaxies became increasingly important. Dressler (1980) has shown that the number of elliptical and lenticular galaxies increases proportionally to the environmental density, while the number of late-type galaxies decreases at the same conditions, see fig. 1.3 (Dressler, 1980; Dressler and Sandage, 1983). Such correlation, the *morphology-density relation*, can be interpreted as evidence of an evolution from late-type galaxies to early-type galaxies, with S0 galaxies once more as a transition type, at least in such dense environments. The mechanisms for such transition would revolve around the removal of the gas content in spiral galaxies infalling towards the centre of clusters due to its interaction with the intracluster gas. Example of such mechanisms include *ram-pressure striping, harassment* or *strangulation* (Gunn and Gott, 1972). If not all the gas of the infalling galaxy is removed, but only a percentage significant enough to halt its star formation rate, we have the *starvation* process (McCarthy et al., 2008), which has almost the same consequences of the ram-pressure stripping to galaxies in dense environments, as a result of this process we would have a galaxy with an old stellar population such as what we see in *early-type* galaxies today. In fact, the fraction of lenticular galaxies in clusters and groups has been shown to decrease with redshift, while the number of spirals increases (Dressler et al., 1997; Wilman et al., 2009). However, van den Bergh (2009) has shown that while S0 galaxies are indeed more common in denser environments, comprising 13% of galaxies in groups and 15% of galaxies in clusters, they also account for 8% of the galaxies in the field. Moreover, the ratio between the amount of S0 galaxies and the other kinds of *early-type* galaxies[1] was found in this same work to account for 33% in clusters, 38% in groups and 34% in fields. If S0s galaxies are formed mostly in denser environments by the transformation of spiral galaxies, we would expect for them to be more prevalent in clusters than in the field, but this seems not to be the case.

In the hierarchical paradigm of galaxy formation, S0 galaxies would be formed from halos of dark matter hosting lumps of baryonic particles, bonded by gravity, that would grad-

[1] As *early-type* galaxies, van den Bergh (2009) considered SA, SO and elliptical galaxies.

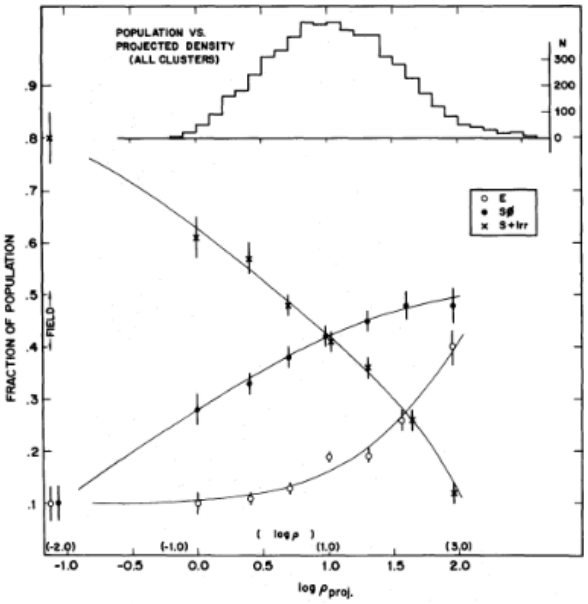

Figure 1.3: Morphology-Density Relation as published in Dressler (1980). The correlation between the environment density, ρ, and the different morphologies is clear. Spiral and Irregular galaxies, shown as crosses, decrease with ρ while S0 (black circles) and elliptical galaxies (open circles) have their number increased in denser environments.

ually form the more complex structures seen today (Hopkins et al., 2010). Observed data from Globular Clusters (GCs) have shown that a two-phase scenario must be taken into consideration as well (Oser et al., 2010). In this perspective, galaxies in most cases would pass through two different phases of star formation: one *in-situ*[2], i.e., the one that happened within the galaxy, and one *ex-situ* that happened in other galaxies or lumps of gas of a primordial gas cloud that then were later accreted by the end galaxy through minor or major merger events (Oser et al., 2010). This second phase is theorised to be able to happen in selected few events or through an extended sequence of minor mergers, such as the cannibalism of dwarf galaxies or globular clusters from neighbouring galaxies.

Simulations indeed have shown that one or several minor mergers are able to form S0s galaxies (Bournaud et al., 2005), while major mergers are expected to form ellipticals. If that is the case, kinematics can play an important role in unravelling clues on the evolution of S0 galaxies, since such events would dramatically affect the kinematics of the stellar populations

[2]The *in-situ* formation of GCs is related to the monolithical collapse theory for galaxy formation (Eggen et al., 1962). In such hypothesis, galaxies and their first GCs are formed from the gravitational collapse of a primordial gas cloud.

and GC systems in such galaxies (Bekki et al., 2005; Coccato et al., 2009; Forbes et al., 2012).

1.2 Kinematics of Discrete Tracers

Classifying galaxies only from their apparent morphologies has several limitations. For instance, in the case of S0 galaxies, if a given galaxy presents itself in edge-on projection, it can easily be mistakenly classified as a spiral galaxy due to its extended disc structure. Moreover, face-on lenticulars are recurrently classified as ellipiticals due to their prominent bulges and the redder colours of their stellar content. Kinematics can be used as a mean of galaxy classification due to the intrinsic kinematical properties of each of the galaxy types proposed by Hubble. Cappellari et al. (2011) proposed a revision of the Hubble sequence by taking into account galaxy kinematics, see fig. 1.4. In elliptical galaxies, the kinematics of their stellar populations are dominated by a larger value of velocity dispersion when compared to the systemic rotation, being therefore kinematically hot systems. S0s and spiral galaxies, however, resemble each other kinematically to some extent by having generally colder kinematics.

Therefore, by studying the kinematics of S0 galaxies, we can better understand how closely related they are from spiral or elliptical galaxies. However, the lack of enough H1 gas in *early-type* galaxies and the fainter stellar light in their outer regions makes it difficult to recover kinematics of such galaxies with the same methods used for *late-type* galaxies (Pota et al., 2013; Brodie et al., 2014; Cortesi et al., 2016). Fortunately, tracers such as GCs or Planetary Nebulae (PNe) can be detected at large radii and provide us with tools to understand the kinematics of their host galaxies as a whole (Bekki et al., 2005; Brodie et al., 2014; Cortesi et al., 2013a).

Recently larger data sets for GCs (Pota et al., 2013) and PNe (Coccato et al., 2009) of S0 galaxies are becoming available, enabling us to study their kinematics in the perspective of the evolution of their host galaxies. The kinematics of PNe is strong related to the one of the overall stellar population of a given galaxy (Coccato et al., 2009; Cortesi et al., 2013a) and therefore can be used to trace stellar kinematics even at large radii, where the surface brightness of stellar light is too low and the imprints of the interaction with other galaxies or

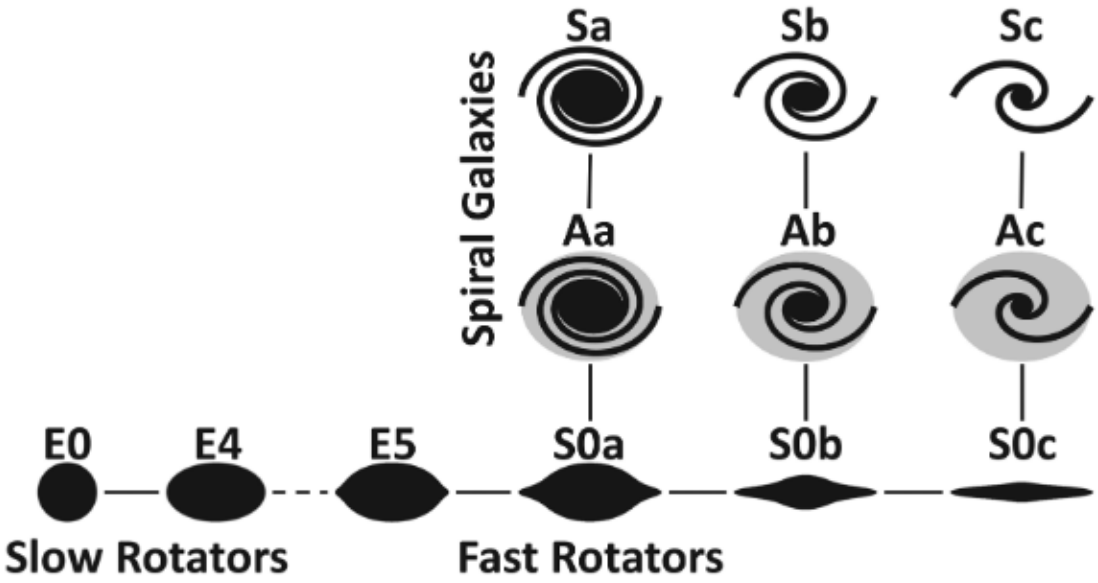

Figure 1.4: Morphology-Kinematics schematics proposed in Cappellari et al. (2011). In this diagram, a revisionism of Hubble's work on fig 1.1, intrinsic kinematic properties of each morphological type of galaxy is taken into consideration. With this perspective, *early-type* galaxies are shown on the bottom, from slow rotators (E0 to E4 elliptical galaxies) to fast rotators (E5 and more flattened ellipiticals, lenticular galaxies). Anaemic Spiral galaxies (Aa, Ab and Ac, van den Bergh (1976)) and regular spirals are shown in a separate category along the fast rotators due to the presence of gas and clearly defined spiral structures on the disc.

the intergalactic medium are stronger. GC kinematics are tightly related to the formation of their host galaxy and past events, such as mergers, in such galaxy evolutionary path (Bekki et al., 2005; Brodie et al., 2014).

1.2.1 Planetary Nebulae

Planetary Nebulae (PNe) are stars at nearly the end of their life cycle that have masses of around $M < 8M\odot$, therefore not massive enough to keep the combustion of heavier elements than hydrogen or helium. In this phase, the star suffers a gravitational collapse in which its outer shell is expelled at velocities that can reach 30 km/s while the star itself collapses into a white dwarf. This outer shell of hot gas constitutes the most prominent part of the PNe and is estimated to last 50,000 years before vanishing into the interstellar medium. The central star, hot and dense, emits UV light that is absorbed and re-emitted by the surrounding gas cloud of the PNe. This emission peaks at around 5007Å, the [OIII] line. As this line is not emitted

by any other source in the interstellar surroundings, PNe are relatively easy to be detected at large galactocentric radii, even in distant galaxies, where they appear only as point-like light sources (Coccato et al., 2009).

Most PNe have ages around $\simeq 1.5$ Gyr (Douglas et al., 2002). Therefore, in the case of early-type galaxies, PNe are expected to be good tracers for stellar kinematics due to its generally old stellar populations. This assumption was confirmed with the advent of specific instruments for extragalactic PNe measurement, such as the Planetary Nebulae Spectrograph (PN.S) and subsequent works that probed the kinematics of the overall stellar populations of galaxies using PNe (Douglas et al., 2002; Romanowsky and SAGES Team, 2013; Noordermeer et al., 2008; Cortesi et al., 2013b, among others).

1.2.2 Globular Clusters

Globular Clusters (GCs) are high density stellar groups that are formed very early in their host galaxy formation, and therefore are very old, with ages > 10 Gyr (Blakeslee, 1997; Forbes et al., 2001; Brodie and Larsen, 2002). Their masses span $10^4 - 10^6 M\odot$ with effective radii peaking around $R_{eff} \approx 4$ pc. In the evolution of galaxies, the GCs we see today are expected to have formed after major starburst events that alter the gas distribution within the primordial galaxy, becoming denser and forming stars in a higher rate than usual (Oser et al., 2010; Brodie et al., 2014). As such, GC dynamics, metallicity and ages can be used to trace back evolutionary events in a given galaxy history. *Early-type* galaxies can host an enormous number of GCs (Brodie and Strader, 2006). M87, the giant elliptical in the centre of the Virgo cluster, is estimated to have over 17 thousand GCs (Oldham and Auger, 2016; Chies-Santos et al., 2011) and lenticular galaxies such as NGC 3115 have over 150 spectroscopic confirmed GCs (Pota et al., 2013; Jennings et al., 2014), to mention a few examples. Star clusters are expected to be present in all galaxy components whereas globular clusters are not likely to survive for long in galactic discs due to rotation effects (Brodie and Strader, 2006) and thus are expected to be found mostly in the central component of galaxies, the bulge, or in their outermost component, the halo. Therefore, the study of their metallicity, dynamics and age can offer clues on the

evolution of its host galaxy, considering specially its innermost GC population, and also on environmental processes a galaxy has experienced through its history by looking at the GC populations in the halo (Bekki et al., 2005). Radially, GCs are distributed in most cases with the same ellipicity as their host galaxies spheroidal regions, suggesting that at least most of them formed within the galaxy (Brodie and Strader, 2006; Forte et al., 2001; Schuberth et al., 2005), but a fraction of the GC population can result from the accretion of smaller galaxies (Schweizer, 2001).

An important feature of GC populations is the fact that most galaxies display bimodality in their GC population optical colour distribution (Brodie and Strader, 2006). Such bimodality suggests the presence of two distinct GC subpopulations within a galaxy, which would be directly related to its host galaxy evolution. The bluer GC population is generally found in the halo and consist of metal-poor objects, while the redder population, on the other hand, are better tracers of the metal-rich components of galaxies and therefore are related to the bulge, much like stellar populations of early-type galaxies such as ellipticals and the thick discs of spiral galaxies (Cortesi et al., 2013b; Pota et al., 2013). Red populations are expected to show, however, more rotational support than blue populations so their kinematics are more akin to the disc component of some galaxies (Muratov and Gnedin, 2010). Other characteristics, such as mass, age and size do not differ much in between the two populations, while metallicity can show a bimodality in GC populations that follows the colour bimodality (Yoon et al., 2006; Brodie and Strader, 2006; Cantiello et al., 2014). This correlation with metallicity, however, is not universal (Muratov and Gnedin, 2010) and alternative views state that it is possible for a flat, almost unimodal metallicity distribution to be present in a GC population that is bimodal in optical colours. Such a fact becomes clearer when we shift to near-infrared colour distributions, for which the colour bimodality for some galaxies become increasingly less evident or even clearly unimodal, as its the case for NGC 1399 (Blakeslee et al., 2010) and M87 (Chies-Santos et al., 2012).

Moreover, the correlation between GC kinematics and colour bimodality is also not clear, however some interesting results have arisen when S0 galaxies were studied. Forbes et al. (2012) studied the galaxy NGC 2768 and found that the red GC population follows the radial

density distribution of bulge starlight and PNe being also kinematically compatible to the bulge stars, while no rotation was found for its blue GCs. This galaxy will be revisited in this work. In the same vein, for NGC 1023, another S0 galaxy, blue GCs show some rotation this time but have kinematics closer to halo PNe and starlight (Cortesi et al., 2016). Bulge-disc decomposition has a very important role in this subject, since with its help we are able to trace the kinematics of GCs of S0 galaxies to different components of the host galaxy. For this objective, however, we need to employ some method to correlate objects to different components of a galaxy. For this extent, in this work we employ a method based on photometry and kinematics.

1.3 This Work

The evolution and assembly of lenticular galaxies in different environments is a great topic of debate and research in contemporary astrophysics. The limitations of using common methods for kinematics analysis in such gas-poor galaxies at large distances makes GCs and PNe excellent and needed kinematic tracers. Specially at large radii, where interesting events in S0 galaxies evolution histories should leave imprints and stellar light is too faint. This work intends to explore these tracers using a maximum likelihood estimation method to statistically infer the best velocity profile for a given galaxy. Combined with photometry, we can also analyse the different subcomponents of a galaxy and its multiple GC subpopulations spatially within the galaxy.

The method used here was first introduced by Cortesi et al. (2011, hereafter C11), when it was applied to PNe of a set of early-type galaxies. Later, in Cortesi et al. (2013b, hereafter C13b), Cortesi et al. (2016, hereafter C16) the lenticular galaxy NGC 1023 was studied, but this time with the addition of a GC sample alongside its PNe. These works revealed the maximum likelihood estimation (MLE) to recover the kinematics of such tracers as a powerful tool to study the evolution of early-type galaxies, such as S0s. The galaxy sample used in those works was small and needed to be expanded, since the only galaxy with its GCs and PNe studied at the same time so far is NGC 1023. This is where the present work

comes along, applying the same method used in C16 to a wider set of S0 galaxies in different environments: NGC 2768, an isolated galaxy, NGC 3115, a group galaxy and NGC 7457, a field galaxy.

This work is divided as follows: In sec. 2 we present the data we used and the different sources from where it was obtained, along with information about the galaxies in our sample; in sec. 3 we present and discuss the MLE method and how we apply it to our sample; in sec. 4 we show the results obtained from this work and discuss the implications of those in the wider range of scenarios proposed in the literature for the evolution of lenticular galaxies and in sec. 5 we summarise our results and present future prospects following the results obtained here.

Chapter 2

Data

In this work, we used spectroscopic and photometric data from GCs and PNe to model the kinematics of a sample of three nearby S0 galaxies. In this section we describe this data and briefly discuss the basic properties already studied in the literature for the galaxies in our sample. In table 2.1 we summarise the size of the samples used for GCs and PNe for each galaxy.

2.1 PNe data and The Planetary Nebulae Spectrograph (PN.S)

The PNe data for the galaxies present in this work was obtained with The Planetary Nebulae Spectrograph (PN.S) (Douglas et al., 2002) and is described and published in C13a[1]. The PN.S is a dedicated instrument mounted at the William Herschel Telescope (WHT) in La Palma, Spain. The instrument detects PNe using a technique based on counter-dispersed imaging (CDI), which enables us to obtain velocities and positions for PNe at the same time. The technique consists in taking, simultaneously, two images of the same field through a slitless spectrograph equipped with an [OIII] filter. The light is then dispersed in two opposite direc-

[1] The PN.S data is publicly available and can be downloaded from: `https://www.strw.leidenuniv.nl/pns/PNS_public_web/PN.S_data.html`

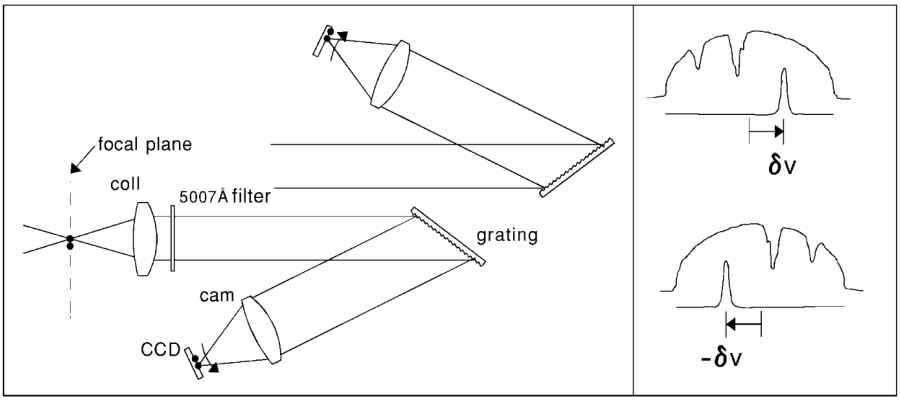

Figure 2.1: Counter-dispersed imaging (CDI) for PNe detection, from Douglas et al. (2002). *Left*: Schematics of CDI imaging; *right*: examples of obtained spectra from both CCDs for stars (spectrum segment) and PNe (single peak emission line). By taking into consideration the displacement δv in the two images, velocities are obtained for the PNe. This plots were taken from Douglas et al. (2002).

tions reaching two different CCDs. The result is that in the final image, stars appear as short segments of spectrum, while PNe appear as point sources due to their concentrated emission at the [OIII] line. By comparing the displacement of the PNe [OIII] emission line in the images of both CCDs, one can readily obtain the relative velocities which later are converted into absolute values in the calibration process (see Douglas et al. (2002) for further details). In fig. 2.1 a schematic representation of the CDI technique is described and in fig. 2.2 a picture from the PN.S instrument is shown.

The PN.S instrument was designed specifically to acquire spectroscopic data from the [OIII] line at 5007Å, which provides an optimal efficiency on targets up to 25 Mpc in distance. The spectroscopic measurements obtained with the instrument have uncertainties of around 20 km/s and are better suited for outer regions of galaxies, due to the difficulties in detecting PNe closer to the centre of galaxies where their light is diluted on a stronger background light from stars. Therefore, completeness and purity estimations and proper corrections are needed in order to take into consideration the many complications in detecting PNe at the inner regions of galaxies or the effects of foreground stars. In C13a, the analysis of incompleteness for the samples used in this work was performed following the method described in Coccato et al. (2009), and resulted in good agreement between the radial density of the PNe and the surface brightness profiles of the host galaxies as obtained with IRAF/ELLIPSE (Jedrzejewski, 1987).

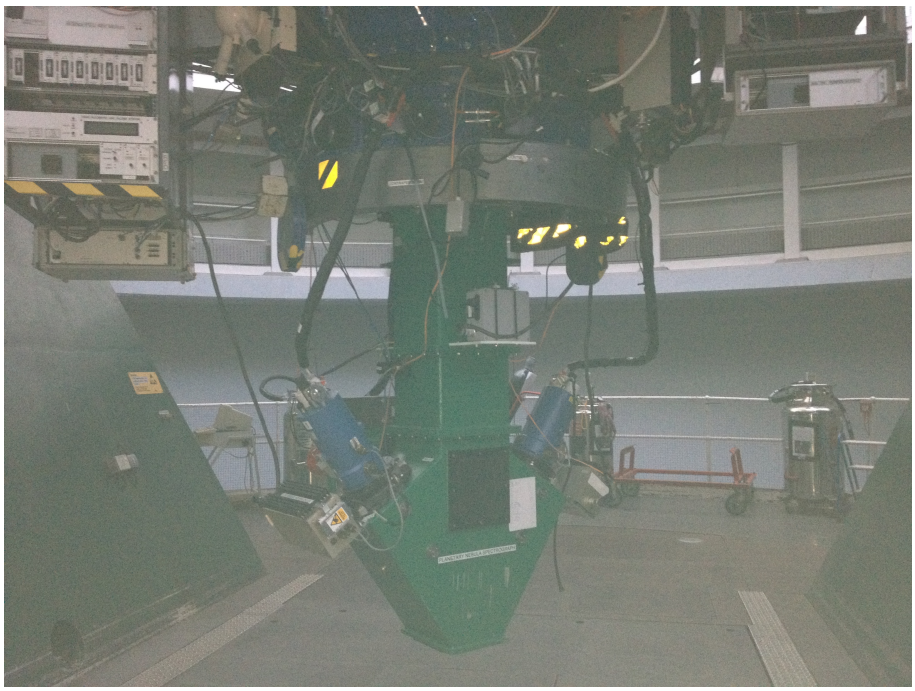

Figure 2.2: Actual PN.S instrument. The light comes from above and is dispersed towards the blue arms on the sides, reaching two CCDs at the end of each one. Credits: Ana Chies Santos.

These results are shown in fig. 2.3, which is taken from C13b.

2.2 GC data and The SLUGGS Survey

The globular cluster photometric and spectroscopic data present in this work comes from The SAGES Legacy Unifying Globulars and GalaxieS (SLUGGS) Survey (Brodie et al., 2014; Forbes et al., 2017). SLUGGS is a wide-field spectroscopic and photometric survey of early-type galaxies using mainly the Subaru/Suprime-Cam imager and the Keck/Deimos spectrograph. SLUGGS goals revolve around studying, with unprecedented detail, the outer regions of early-type galaxies, where stellar light is fainter. Photometrically the survey has *gri* deep imaging of 25 nearby early-type galaxies, and near-infrared Ca II triplet (CaT) measurements that provide spectroscopy for selected targets within the photometric catalogues.

Observations of all galaxies present in this work have been described in Pota et al. (2013). NGC 2768 was observed with the Suprime-Cam instrument of the Subaru telescope which has a field of view of 34 x 27 arcmin and a pixel scale of 0.202 arcsec (Miyazaki et al.,

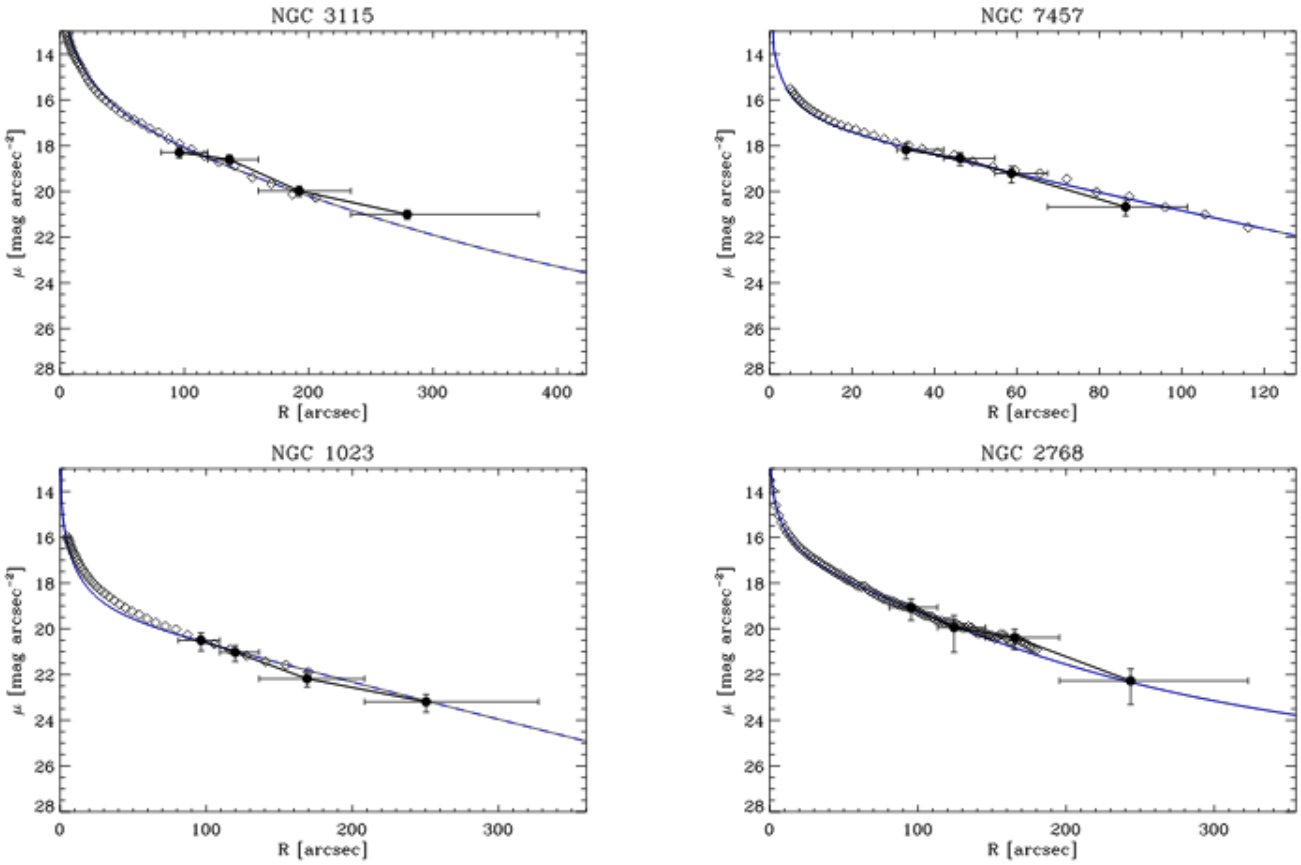

Figure 2.3: Comparison between PNe radial density and surface brightness profiles fitted using IRAF/ELLIPSE, published in C13b, for our sample galaxies and NGC 1023, after incompleteness corrections. Diamonds represent the ELLIPSE fit, filled circles represent PNe number density and the blue lines represent the extrapolation of a Sérsic profile plus an exponential disc profile fitted for the galaxies' light profiles.

2002). Additional photometric information for this galaxy comes from the SMOKA archives (Baba et al., 2002) and the Advanced Camera for Surveys (ACS) from the Hubble Space Telescope (HST), obtained from the Hubble Legacy Archive and described in Pota et al. (2013). Spectroscopy for this galaxy was obtained using the DEIMOS spectrograph from the Keck-II-Telescope (Faber et al., 2003) with a field of view of 16x5 arcmin and CaT absorption line Doppler shift measurements.

NGC 3115 data is described in details in Arnold et al. (2014). Observations for this galaxy were obtained with the Subaru/Suprime-Cam, with spectroscopy from Keck/DEIMOS, and additional spectra from the LRIS instrument on the Keck-I-Telescope, with a field of view of 6x7.8 arcmin (Oke et al., 1995) and the IMACS instrument from the Magellan telescope (Dressler et al., 2011).

The photometric GC data for NGC 7457 included in SLUGGS comes from Hargis et al. (2011), obtained from observations in the *BVR* filter with the WIYN/MiniMo imager (Saha et al., 2000). Hargis et al. (2011) also obtained spectroscopy for a sample of 20 NGC 7457 GCs, however, in this work we use an updated and larger spectroscopic sample for this galaxy's GCs obtained with the KECK/DEIMOS spectrograph and published on Forbes et al. (2017). This new sample has spectroscopy for 40 GCs, which is double the amount previously published. However, only 22 GCs are present in both Hargis et al. (2011) photometric catalogue and Forbes et al. (2017) spectroscopic sample. The main interest for studying this galaxy is on velocity measurements of a sample of its GCs, therefore we adopted this larger sample and discuss in section 4.5 the implications of this decision on the final results.

As in this dissertation we employ a maximum likelihood estimation (MLE) for GCs and PNe of our sample galaxies, the size of the samples are important to some extent to ensure good results. Further details on the efficiency of the method will be fully explored in chapter 3, but we note that in C13b it is shown that the MLE method is able to obtain reliable results even with somewhat smaller samples, as its the case of NGC 7457. Therefore, we expect larger uncertainties in the estimation of the kinematic parameters for this galaxy GCs, when compared to the same procedures for NGC 2768 and NGC 3115 GCs, but we don't expect systematic

Galaxy	N_{GC} Photometric	N_{GC} Spectroscopic	N_{PNe}
NGC 2768	978	106	315
NGC 3115	781	150	188
NGC 7457	536	40	112
NGC 1023	360	115	203

Table 2.1: Size of GC and Planetary Nebula samples used in this work for our sample galaxies with the addition of the amount of the same tracers used in C16 for NGC 1023, for comparison purposes throughout this work. In the second column we have the number of the GC sample for each galaxy for which only photometry is available, in the third column we have the number of GCs for which spectroscopy data is available and in the last column the number of PNe available for each galaxy (with spectroscopic and photometry obtained simultaneously in the PN.S). See section 2.1 and 2.2 for further details on each sample.

errors that could compromise the fit. In what concerns the other galaxies, their GC and PN sample sizes are comparable in size to the ones used for a successful application of the method for NGC 1023, so we expect similarly satisfactory results.

2.3 Images used for the spheroid-disc decomposition

In this work we implement spheroid-disc decomposition for our sample galaxy images by fitting surface density profiles using GALFIT (Peng et al., 2002). This procedure is described in detail in section 3.1. The images used for our sample galaxies are K-band images from 2MASS (Skrutskie et al., 2006).

2.4 Galaxies Present In This Work

In this section we present the general properties of the galaxies studied here. In table 2.2 these properties are summarised, and the multiple sources used to gather such information is referenced. In the next subsections we discuss briefly other interesting properties and past studies on our sample galaxies and NGC 1023.

Galaxy	Dist. (Mpc)	V_{sys} (km/s)	σ_{sys} (km/s)	ϵ	env.	morph.	Age (Gyr)	R_e (kpc)	$log(M_*)$ (M$\odot$)
NGC 2768	21.8	1353	206	0.57	G	E/S0	12.3	6.37	11.21
NGC 3115	9.4	663	248	0.66	F	S0	9.0	1.66	10.93
NGC 7457	12.9	844	74	0.47	F	S0	3.8	2.13	10.13
NGC 1023	11.1	602	183	0.63	G	S0	12.3	2.58	10.99

Table 2.2: General properties of our sample galaxies and NGC 1023 published in Alabi et al. (2017). From left to right, the columns are: Galaxy designation, distance, systemic velocity, central stellar velocity within 1 kpc, ellipticity, environment (F=Field, G=Group), galaxy morphology from Brodie et al. (2014), average luminosity-weighted age of the stellar population within 1 R_e from McDermid et al. (2015), effective radius and stellar mass.

2.4.1 NGC 2768

NGC 2768 is a group galaxy classified as an E6 by de Vaucouleurs et al. (1991) and S0 1/2 by Sandage and Bedke (1994), located relatively nearby with a distance of about 22 Mpc from us (Tully et al., 2013) in the direction of the constellation of Ursa Major. It is part of the Lyon Group of Galaxies 167 (Garcia, 1993), and has traces of ionised gas and a dust lane along the minor axis (Kim, 1989). It is interesting to add that the ionised gas and stars in the inner regions of the galaxy have been found to have different kinematics (Fried and Illingworth, 1994). Pota et al. (2013) found a bimodal distribution in colour for the sample of 978 GCs used in this work with a separation at $(Rc - z) = 0.57mag$, obtained with KMM (Ashman et al., 1994).

This galaxy's red subpopulation of GCs has already been studied with a method similar to the applied here by Forbes et al. (2012). They found that the red GCs follow the radial surface density profile and are compatible with kinematics of the bulge component of the galaxy. Pota et al. (2013) finds rotation for the red GCs of this galaxy and no rotation for the blue subpopulation.

2.4.2 NGC 3115

NGC 3115 is the closest S0 galaxy to us, with a distance of 9.8 Mpc (Cantiello et al., 2014) and shows the most clear bimodality of our sample (Brodie et al., 2012; Pota et al., 2013; Cantiello et al., 2014; Arnold et al., 2014). Pota et al. (2013) found a colour separation for our sample of photometric GCs at $(g - i) = 0.91mag$.

This galaxy is located in the field (Brodie et al., 2014) and displays many interesting morphological structures, such as spiral structures proposed by Norris et al. (2014) and redetected recently using VLT/MUSE spectroscopy by Guérou et al. (2016). It has two faint companion galaxies (Doyle et al., 2005).

2.4.3 NGC 7457

NGC 7457 is a field S0 galaxy (Brodie et al., 2014) with a distance of 12.1 Mpc from us (Tully et al., 2013) that, as opposed to the other galaxies in our sample, shows no signs of bimodality in its GC population (Hargis et al., 2011; Pota et al., 2013). Previous studies with this galaxy also proposed a counter-rotating galaxy core (Sil'chenko et al., 2002) and a possible merger origin (Hargis et al., 2011). Furthermore, it presents the least amount of GCs of all galaxies in our sample, with a total number of $\sim 210\pm 30$ GCs, which is consistent with the total number of GCs in late-type galaxies, such as M31 and the Milky Way (Hargis et al., 2011).

2.4.4 NGC 1023

NGC 1023 is a group S0 galaxy at a distance of 11.1 Mpc from us (Alabi et al., 2017). This galaxy has an interacting companion galaxy, NGC 1023A (C16) and shows colour bimodality for its GC population with a separation at $(g-z) = 1.1mag$ (Forbes et al., 2014). In C16, kinematic analysis of its GCs and PNe has shown rotation on both blue and red subpopulations of GCs and a discrete amount of GCs with disc-like kinematics. Further analysis of the results obtained for this galaxy on C16 will be discussed throughout this work and compared with the results obtained for our sample galaxies. NGC 1023 is so far the only other galaxy for which this method was applied for its whole GC and PNe populations, so it is invaluable to the comprehension of the results obtained here.

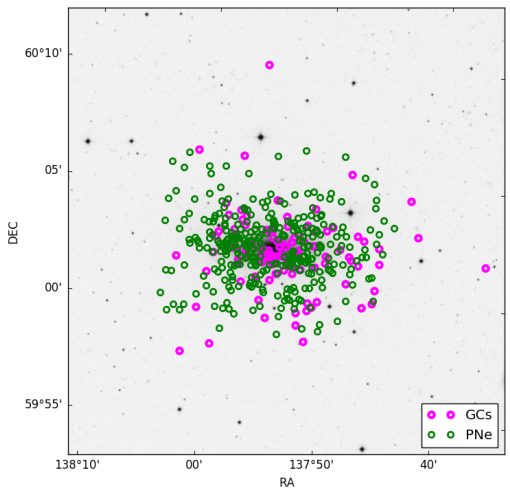

(a) NGC 2768

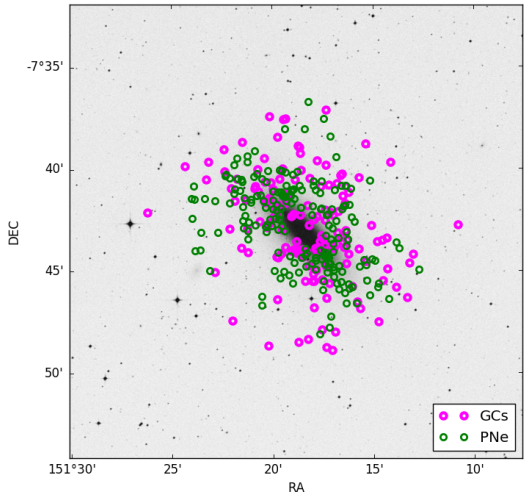

(b) NGC 3115

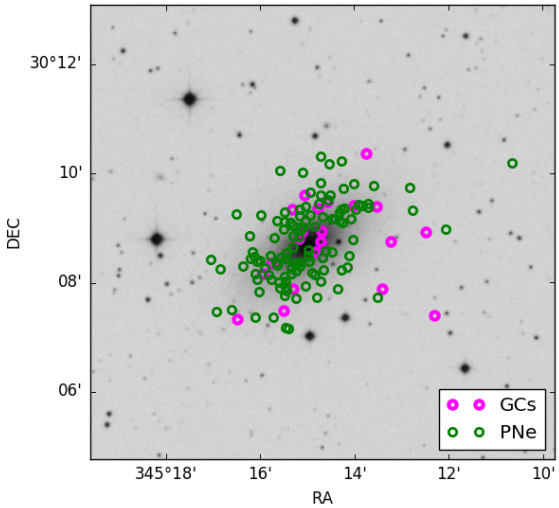

(c) NGC 7457

Figure 2.4: Positions of planetary nebula and spectroscopic GC samples described in this section for our sample galaxies, overplotted in the k-band images from 2MASS used for the spheroid-bulge decomposition.

Chapter 3

The Kinematic Likelihood Method

In this section we present the method used in this work to analyse the kinematics of GCs and PNe belonging to our sample galaxies, and how we may use this information to learn more about these galaxies' evolutionary histories. Regular photometric techniques have several limitations for the purpose of studying the evolution of galaxies, especially lenticulars. Some of those drawbacks are: the faintness in surface brightness of the outer regions of galaxies, preventing one to probe clues of the interaction between the galaxy and the environment with only photometry; the generally smaller amount of gas content in lenticulars when compared to spirals, complicating the recovering of the galaxy kinematics from H1 gas, for instance; or the general difficulties in overcoming projection effects that often lead to lenticulars being mistakenly classified as ellipiticals. Therefore, kinematics has an important role as a tool to study properties associated with galaxy evolution that are otherwise harder to obtain. However, due to the nature of S0 galaxies, as stated before, we cannot rely solely on the galaxy light or gas to recover kinematic profiles. We focus instead in analysing discrete kinematic tracers, such as GCs and PNe. Extragalactic GCs and PNe can be detected at distances up to 100 Mpc (Harris, 2010), and at radii up to $\sim 5R_e$ of their host galaxies (Brodie et al., 2014), where the galaxy light is too faint for conventional photometry. PNe have been shown to be excellent tracers of the kinematics of the global stellar population of their host galaxy (Napolitano et al., 2001; Coccato et al., 2009; Cortesi et al., 2013a) and the kinematics of GC systems is tightly

correlated to past events in the host history of the host galaxy, such as mergers and other formation scenarios proposed for S0 galaxies (Bekki et al., 2005; Bournaud et al., 2005).

To analyse the kinematics of GCs and PNe of a given galaxy, a useful and powerful method was developed in C11 and C16 and is applied in this dissertation. Basically, the method can be described by the following steps:

- A photometric spheroid-disc decomposition of the galaxy light is performed with software such as GALFIT (Peng et al., 2002);
- The spheroid model obtained with GALFIT is divided from the total model of the galaxy light, to obtain what we call the *f-map*, which is then used to estimate the probabilities, f_i for the GCs to belong to the spheroid of the galaxy only by its apparent positions over the galaxy image.
- The GC velocity distribution is then modelled as a single gaussian model with mean velocity V and a dispersion velocity σ, obtained through Maximum Likelihood Estimation (MLE).
- Finally, using the f_i probabilities for the GCs and the previously obtained velocity distribution functions of the PNe of each of our sample galaxies, obtained with the same *f-map* procedure and MLE fit as used in this work, published in C13b, the probability for each GC to belong to the galaxy disc or spheroid can be now calculated from a kinematic perspective, which we expect to improve the probabilities obtained only with photometry.

To complement this methodology, we also employed a few other procedures in this work, such as comparing the GC radial density profiles with the modelled light profiles obtained with GALFIT, statistical smoothing of the velocity maps from our spectroscopic GC samples and an analysis to look for correlations between the colour subpopulations of GCs and the results we obtained from the kinematic fit. These extra steps were needed to confirm that PNe kinematics can be used to describe GC kinematics, while also gathering additional information on the GC samples.

3.1 Photometric Spheroid-Disc Decomposition

The first phase of the method consists in applying a photometric spheroid-disc decomposition on a galaxy image. In general, lenticular galaxies are well modelled as a combination of a disc component and a spheroid, comprising a bulge and a halo. There are 1D decomposition routines that only account for fitting the light profile of the galaxy, and 2D routines that, given an image of a galaxy, fit the surface brightness profiles in a more precise way. In general, a combination of Sérsic functions (eq. 1.1) is used to model the different components of a galaxy (Caon et al., 1993). Several routines exist to perform such decomposition numerically, such as IRAF/ELLIPSE in 1D, GALFIT (Peng et al., 2002) and MegaMorph (Vika et al., 2013) in 2D, to name only a few. In this work, we have used the quantities obtained using GALFIT, in C13b, for the light profiles of the galaxies in our sample.

In C13b, images of each galaxy were decomposed in disc and spheroid, obtaining estimated values for the light profiles of such components. These are listed in table 3.1. It was adopted a Sérsic profile to model the spheroid light for our galaxies and an exponential disc profile to model the disc. For all galaxies in our sample, K-band images from 2MASS have been used to perform the decomposition. This modelling, with a disc and a spheroid, comprising bulge and halo as previously mentioned, works well in general for S0 galaxies and for the purpose of this work. However, it is to be noted that some galaxies have slightly more complex structures. NGC3115, for instance, shows signs of multiple disc features that closely resemble spiral arms, as noted by Norris et al. (2006). Nonetheless, for the scope of this work, this spheroid-disc modelling is good enough for recovering the kinematics of the galaxy as it was shown on C16.

Table 3.1: Light profiles estimated parameters for sample galaxies, from Cortesi et al. (2013b) and used for the analysis in this work. [1] disc apparent magnitude, [2] disk scale lenght, [3] axis ratio, [4] galaxy inclination, [5] position angle, [6] spheroid apparent magnitude, [7] effective radius, [8] sérsic index n for spheroid, [9] axis ratio of the spheroid, [10] position angle fitted for the spheroid.

	Disk					Spheroid				
Galaxy	m_D (mag)	R_D (arcs)	b/a	$incl$ (deg)	PA (deg)	m_B (mag)	R_e (arcs)	n	b/a	PA (deg)
NGC 2768	8.19	42.93	0.29	73.0	-86.25	7.23	50.46	4.65	0.66	-85.39
NGC 3115	8.34	53.69	0.39	67.0	45.00	7.17	26.19	4.00	0.31	45.0
NGC 7457	8.56	27.07	0.48	62.0	-57.28	9.49	11.62	4.00	0.62	-46.04

3.2 GC radial density and the fitted surface brightness profiles

To both verify the consistency of the models obtained above and to analyse how the GCs for our galaxies are distributed along the galactocentric radius, we proceed to compare the obtained light profiles with the radial photometric GC density for our sample galaxies (see figure 3.1). Since the light of the galaxy is mainly due to stars, this plot is able to show us, in a basic and preliminary way, how GCs are correlated to the general stellar population of our sample galaxies. Also, the spheroid-disc decomposition allows us to further enhance this analysis by looking at how much the light profiles of separate components of the galaxy are compatible with the GC density, hinting at which of the host galaxy's components its GCs are better correlated with. For comparison purposes, we add in fig. 3.1 the GC density and the light profiles for NGC 1023 published on C16.

Moreover, we separately calculated the GC colour subpopulations radial density for NGC 2768 and NGC 3115. For NGC 7457, similar to what is done for all other plots in this work, only the total GC population of this galaxy was taken into consideration due to its lack of detected colour bimodality. Pota et al. (2013) performed tests on the colour bimodality of our sample galaxies using gaussian mixture modelling (GMM). The values obtained in that work are used here to separate GCs into colour subpopulations. Furthermore, this same work also shows that the GCs of NGC 7457 do not display significant colour bimodality. We proceeded by dividing the photometric GCs for each galaxy into elliptical bins with approximately the

same number of GCs in each bin and the same ellipticity of the host galaxy, with the first bin starting at the position of the GC with the smallest galactocentric radius. The final GC density was calculated by dividing the number of GCs for each bin by the bin area. The number of bins was determined by the size of the GC photometric sample of each galaxy, to ensure we get a reasonable amount of objects in each bin.

For NGC 2768, the GC radial density profile shows good agreement, within errors, with the spheroid light. At least visually however, the agreement between the disc light and GC density is not as strong, though. In fig. 3.1 (c), the radial density for the photometric GCs of NGC 7457 also displays good agreement with both spheroid and disc modelled profiles. These preliminary results will be shown later to be consistent with the kinematic analysis (see section 4.7).

For NGC 3115, the modelled light profiles do not show such strong agreement with GC density as previously seen for NGC 2768 and NGC 7457. This could be a consequence of the aforementioned difficulties in fitting this galaxy with a spheroid and disc model, although as seen in fig. 2.3, PNe show good agreement with the galaxy light nevertheless. Fortunately, our modelled profiles seem to be a reasonable approximation given the simplicity of our starting model. The density of GCs appears to have a slightly stronger correlation with disc light except at large radii. Such result will also be revisited after the kinematic analysis (see section 4.7).

Comparing to the same plot for the NGC 1023, from C16, we can see that the good agreement between light profiles and GC radial densities is also present.

3.3 f-map

After the spheroid-disc decomposition, by dividing the spheroid model from the total model of the galaxy light, we obtain an *f-map*, which is used to get preliminary probabilities f_i for each GC to belong to the spheroid region of the galaxy, based on their position over the galaxy image.

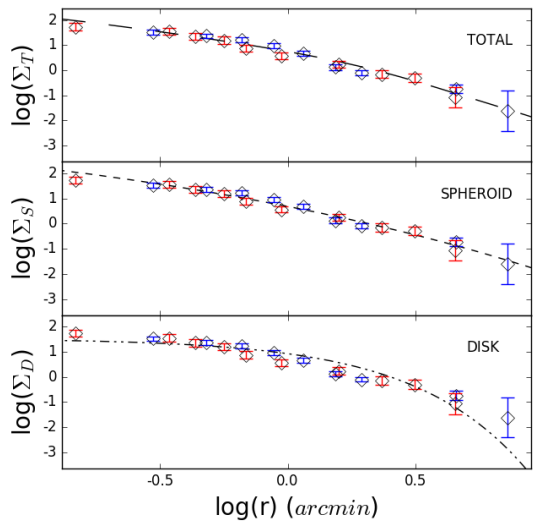

(a) NGC 2768

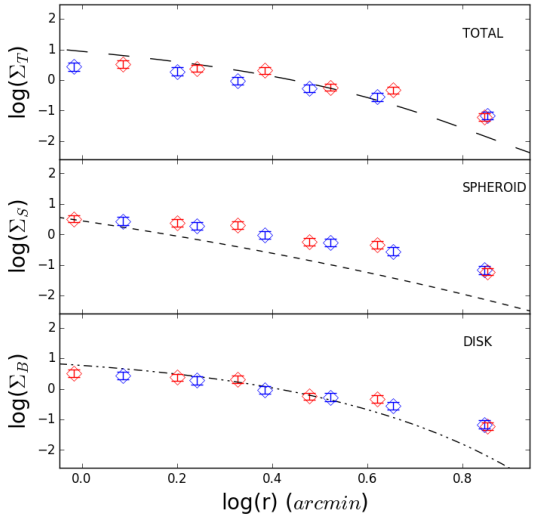

(b) NGC 3115

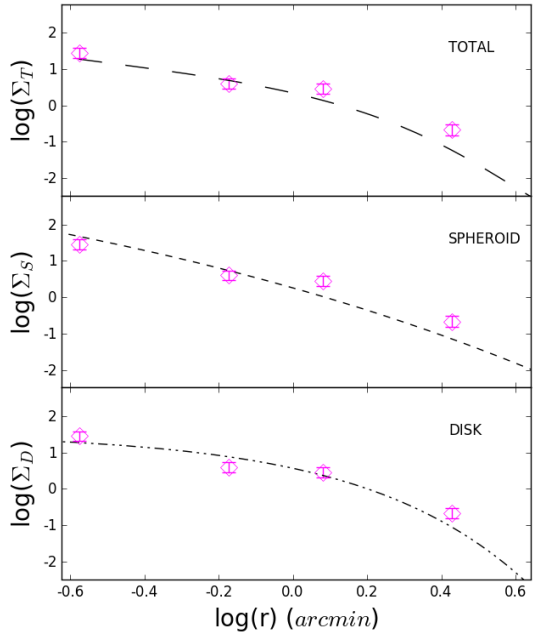

(c) NGC 7457

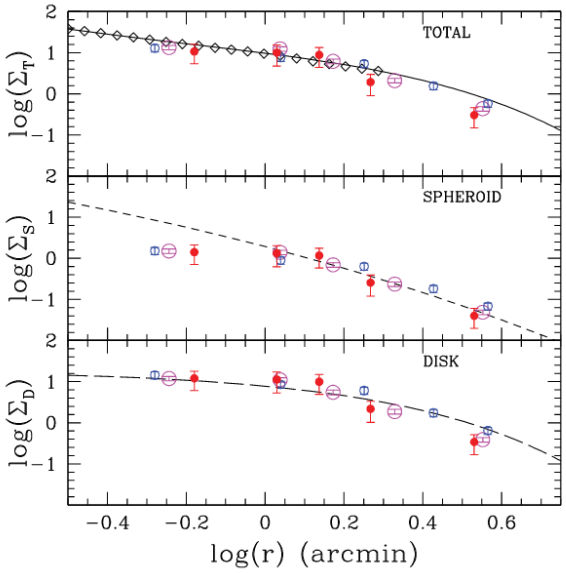

(d) NGC 1023

Figure 3.1: GC radial density and sample galaxies surface brightness profiles as shown in sect. 3.1. GC colour subpopulations are colour-coded by their respective colours. For NGC 7457 only the total population of GCs is shown with magenta open circles. On the bottom right panel, we add this analysis for NGC 1023 published in C16, where open magenta circles represent the total GC population, blue open circles and red filled circles represent blue and red GC subpopulations respectively. Also, for NGC 1023, open diamonds represent the surface brightness fitted with IRAF/ELLIPSE for comparison with the GALFIT fit of an R-band image of the galaxy. Σ_T, Σ_S and Σ_D represent the surface brightness profiles for the total galaxy light, spheroid and disc, respectively.

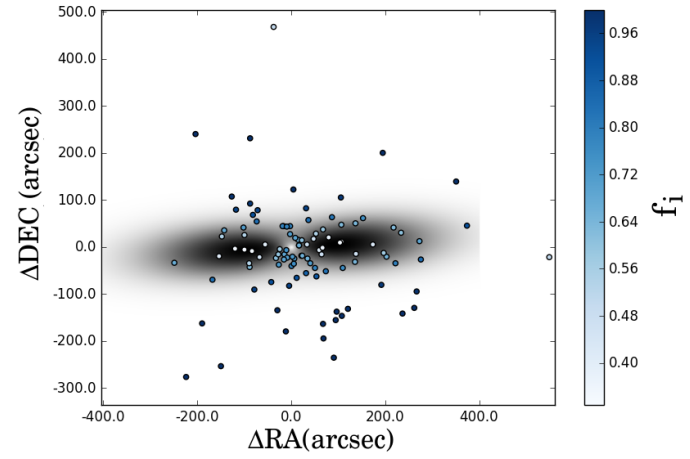

(a) NGC 2768

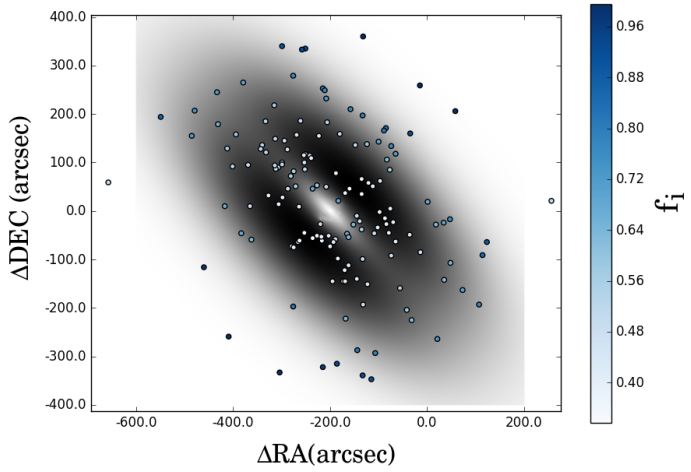

(b) NGC 3115

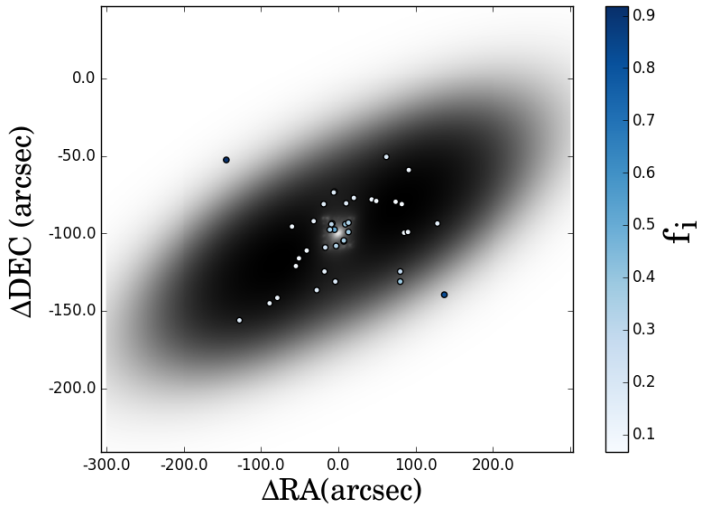

(c) NGC 7457

Figure 3.2: *f-map* for sample galaxies. The spheroid model obtained with GALFIT is divided from the total image of the galaxy and f_i values are assigned to each GC representing the probability of belonging to the spheroid based only on its position over the divided image.

- $f = 1$ means that the object certainly lies on the spheroid;
- $f = 0$ means that the tracer certainly belongs to the disc.

As discussed in section 3.1, we adopted in our analysis the GALFIT results from C13b, therefore the *f-maps* used in this work to calculate the f_i values for GC are the same that were used in C13b to obtain such probabilities for PNe of our sample galaxies. We present these *f-maps* in fig. 3.2, with our samples of spectroscopic GCs overplotted and colour-coded by each individual value of f_i obtained. Objects that are located outside of the image area are assigned an f_i value of 0.5. See C13b for more details on this procedure.

The values of f_i will be used as preliminary information on the probability of a GC to belong to each component of the galaxy, but are obviously prone to systematic errors due to projection effects. Therefore, the MLE fitting and the recalculation of such probabilities with kinematic information is expected to be able to reduce drastically the influence of such projection effects and thus improve our results.

3.4 Preliminary Kinematic Properties

In most galaxies, GCs can be separated into two subpopulations based on their colour, namely a red generally metal-rich population and a blue and metal-poor one. Different scenarios have been proposed to explain the evolution of such subpopulations within an evolving galaxy, such as blue globular clusters being formed in the halo (Forbes et al., 1997), with red GCs more associated to the bulge, even if the evolutionary paths that lead them to this scenario involve forming alongside the spheroid or migrating towards the center of the galaxy after a gas-rich phase of galaxy evolution (Shapiro et al., 2010). Two-phase scenarios have also been proposed (Oser et al., 2010) to explain the existence of two subpopulations of GCs as a result of two distinct star formation events in the evolution of most galaxies. Our method aims to describe the kinematics of the GC population of our sample galaxies not only by colour, but also by the probabilities of each GC to belong to each of the host galaxy components.

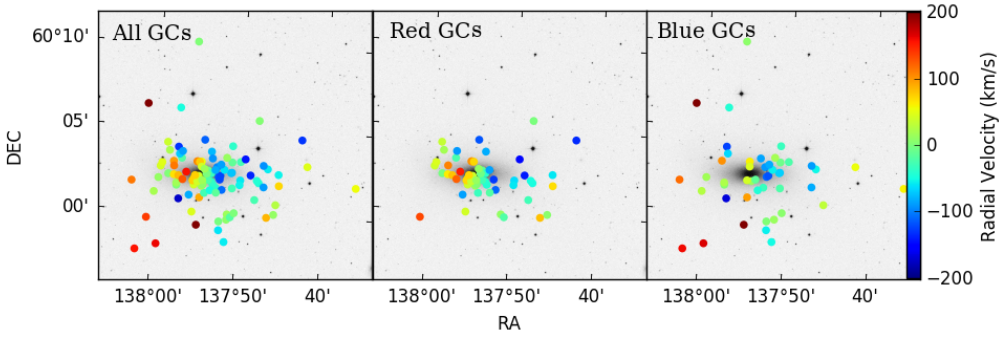

(a) NGC 2768

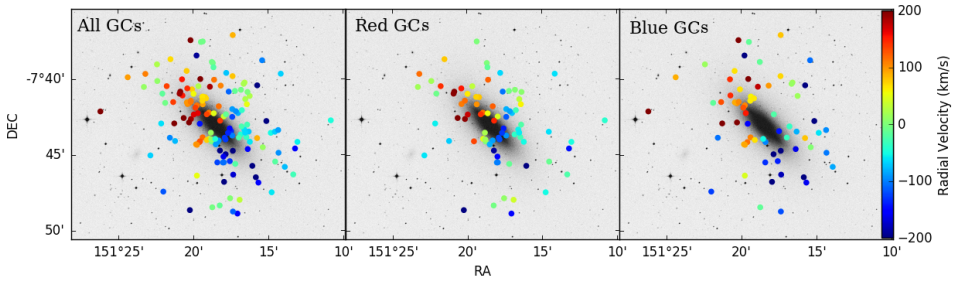

(b) NGC 3115

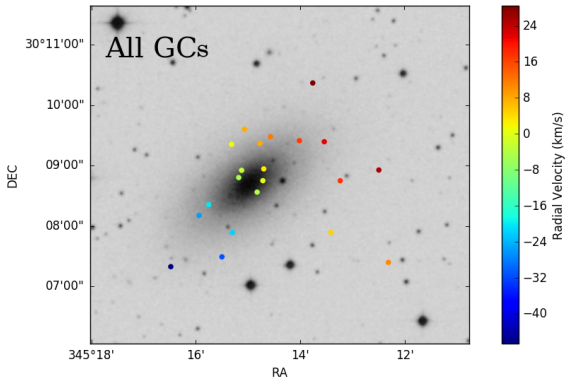

(c) NGC 7457

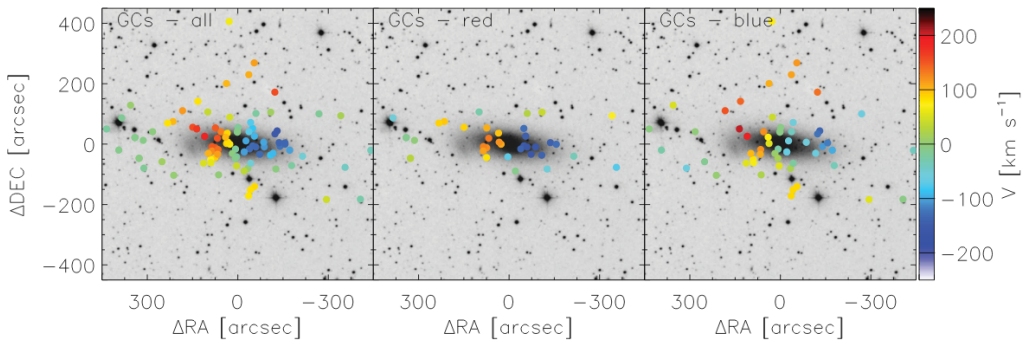

(d) NGC 1023

Figure 3.3: Smoothed Velocity maps of our sample galaxies GC subpopulations, using Adaptive Kernel Smoothing (Coccato et al., 2009). Rotation is detected in all galaxies. On the bottom panel, we add the smoothed velocity map for NGC 1023 GCs published in C16.

Galaxy	A	B (arcsec)
NGC 2768	0.38	250.85
NGC 3115	0.45	184.19
NGC 7457	0.87	38.92

Table 3.2: A and B parameters for our sample galaxies AKS proceeding to obtain smoothed velocity maps.

As a first approach to the kinematics analysis, we analyse the spatial distribution of the kinematics of the GC colour subpopulations of our sample galaxies. To this extent, we apply the method of Adaptive Kernel Smoothing (AKS), developed in Coccato et al. (2009). AKS makes use of a Gaussian Kernel to approximate the actual observed velocity distribution of the GC samples into a more visually smoothed and clear distribution. This enable us to avoid the interference of kinematic outliers that pollute the globular cluster velocity maps and more clearly see the rotation pattern that such systems exhibit in a given galaxy. A complete description of the method is available in Coccato et al. (2009). Here we briefly describe how we specifically applied the method to our data.

Given a set of objects with positions (x_p, y_p) and velocities v_i, we compute new velocities $\tilde{V}$ with the following form,

$$\tilde{V}(x_p, y_p) = \frac{\sum_i v_i w_{i,p}}{\sum_i w_{i,p}}, \tag{3.1}$$

where w_i is a distance-dependent weight for the ith object defined by:

$$w_{i,p} = exp\frac{-D_i^2}{2k(x_p, y_p)^2}, \tag{3.2}$$

where k is the gaussian kernel amplitude and D_i is the distance from the ith object to (x_p, y_p). The amplitude k varies from galaxy to galaxy and is defined by:

$$k(x, y) = AR_m(x, y) + B, \tag{3.3}$$

where $R_m(x, y)$ is the distance from the object with position (x, y) from the closest Mth object. The values of M were arbitrarily set to $M = 20$, but between $M = 10$ and $M = 60$ show no significant influence in the final results (Coccato et al., 2009). The constants A and B vary for each galaxy and need to be set very carefully to ensure that the smoothed velocities are not too distorted from the real measurements of these quantities. To this extent, we have simulated several artificial sets of velocities which resemble the actual observations and by applying this procedure using different values for A and B, we assume that the most reliable values for such constants are the ones that return the best compromise between the kinematic resolution of the original observations and the smoothing, i.e, by minimising the effects of objects with exotic kinematics within the distribution but without completely deforming the distribution enough for us to lose the physical meaning behind it. These values are summarised in table 3.2. Finally, Monte-Carlo simulations have been performed to obtain uncertainties for $\tilde{V}$ and for all galaxies and such uncertainties are of the order of $\Delta V \approx 25$ km/s.

In figure 3.3 we show smoothed velocity maps for each galaxy using the described adaptive kernel smoothing technique, with the addition of NGC 1023 smoothed velocities published in C16. We can clearly see that rotation is present for all GC subpopulations in all galaxies, but notice that, for the case of NGC 2768, the rotation is more evident for the red GCs closer to the center of the galaxy. When we compare this result with that of NGC 3115 or the previous studied NGC 1023, that have clear rotation on both subpopulations, NGC 2768 stands out as an interesting case for having kinematically distinct GC colour subpopulations.

3.5 Likelihood Analysis

In this section we will summarise the method developed in C11; C16 and applied in this work. It consists basically in using maximum likelihood estimation (MLE) to find global kinematic parameters for a given galaxy assuming a gaussian velocity distribution for its GCs or PNe.

Given a set of $v_i = (v_1, ..., v_n)$ values for the velocities of tracers such as GCs or PNe of a given galaxy, we assume they are drawn from a probability density function $F = F(v_i; \theta)$,

where $\theta = (V, \sigma)$ are the parameters we want to estimate. The likelihood function L will then be given by:

$$L = \prod_i F(v_i; \theta). \tag{3.4}$$

The values of V and σ that maximize L are the best estimators for the actual values of these parameters. Given a set of Gaussian distributed independent measurements, such as velocities of GCs and PNe used in this work, the maximum likelihood method can be approximated by the least-squares method and thus has its uncertainty measured by usual χ^2 statistics:

$$\Delta\chi^2(\theta) = -2\Delta lnL(\theta), \tag{3.5}$$

where $\Delta lnL(\theta)$ is the difference between the maximum and minimum values of $\ln L$. Therefore, we can set confidence limits for the best estimators in the form:

$$lnL(\theta) \geq lnL_{max} - \Delta lnL. \tag{3.6}$$

In this work, we are using a 2σ coverage probability, thus we need to use the correspondent value for $\Delta lnL = \Delta\chi^2$ to set the confidence limits around the best estimators θ. Thankfully, these values are already available in tabulated form for a given set of m free parameters. In our case, $m = 2$, so $\Delta\chi^2 = 2.77$.

To obtain our likelihood function $F(v_i, \theta)$, we adopt an inclined disc model for our galaxies, as described in C11. Considering a galaxy model consisting of an inclined rotating disc, the velocity of an object in such galaxy v_i is a projection of the galaxy's mean rotational velocity V, which is part of the line-of-sight velocity of the form:

$$V_{los} = V_{sys} - V sin(i) cos(\phi), \tag{3.7}$$

where such object is at an azimuthal angle on the galaxy plane, ϕ, the inclination of the galaxy to the line-of-sight is i and the systemic velocity of the galaxy itself is V_{sys}. Furthermore, we adopt the simplest possible model for the velocity distribution of such objects, a gaussian distribution with mean velocity V_{los} and dispersion velocity σ:

$$F(v_i;\theta) \propto exp\left[-\frac{(v_i - V_{los}(V)^2}{2\sigma^2}\right]. \tag{3.8}$$

In summary, the values of $\theta = (V, \sigma)$ which maximise the likelihood function L in equation 3.4 are the best estimators for the actual kinematic parameters of the whole GC system of a given galaxy.

In order to apply 3.4 and maximise the likelihood function L, it is convenient numerically to take its negative logarithm, $-ln(L)$, and then find its minimum, which would correspond to the maximum of L. This procedure is also useful since it allows us to directly apply the confidence limits using equation 3.5.

We apply the MLE fit by binning our data in elliptical annuli with the same ellipicity of the disc component for each galaxy (as presented in table 3.1), with approximately the same number of objects but with different bin areas along the galaxy radius. In this way we ensure not to lose information on how the kinematics of our tracers change with radii. Also, we run the MLE fit several times until all objects within the sample used for the estimation are within the 2σ confidence interval, discarding outliers in each run. This ensures the reliability of the fit even when dealing with a possible significant number of outliers.

3.6 Final probabilities from photometry, kinematics and PNe

In C13b, kinematics of PNe for all galaxies in our sample were modelled using this same MLE fitting process but with a likelihood function $\mathcal{L}$ which combines the contribution from

the kinematics of the spheroid (bulge and halo) and the disc component of a given galaxy. Since PNe are expected to be good tracers of the overall stellar population of the host galaxy (Coccato et al., 2009; Cortesi et al., 2011), by calculating the probabilities of GCs with the velocity distribution function obtained with PNe, we can infer how they are distributed in each component of the host galaxy. In this section we summarise the model used for the MLE fit of the PNe kinematics for our sample galaxies published in C13b. The likelihood function used has the following form:

$$\mathcal{L}(v_i; V, \sigma_r, \sigma_\phi, \sigma_{sph}) \propto \frac{f_i}{\sigma_{sph}} exp\left[-\frac{v_i^2}{2\sigma_{sph}^2}\right] + \frac{1-f_i}{\sigma_{los}} exp\left[-\frac{(v_i - V_{los})^2}{2\sigma_{los}^2}\right]. \tag{3.9}$$

For the spheroidal kinematics, we have adopted a gaussian velocity distribution with zero mean velocity and velocity dispersion σ_{sph}. We assume, therefore, a kinematically hot spheroid expected to be dominated by random motions. For the disc kinematics, the same inclined disc model from C11 was adopted, where an object velocity v_i is a projection of the galaxy's mean rotational velocity V, as described by eq. 3.7. The velocity dispersion in the disc, however, is expressed in cylindrical coordinates (R, ϕ, z), so that it can be quantified in different directions: σ_r, σ_ϕ and σ_z. Therefore, the line-of-sight velocity dispersion σ_{los} for objects in the disc has the following form:

$$\sigma_{los}^2 = \sigma_r^2 sin^2(i) sin^2(\phi) + \sigma_\phi^2 sin^2(i) cos^2(\phi) + \sigma_z^2 cos^2(i). \tag{3.10}$$

Due to the fact that all galaxies in our sample are nearly edge-on, σ_z will have negligible significance and therefore can be ignored in equation 3.10. We are then left only with the radial and azimuthal contributions to σ_{los}. These components vary sinusoidally, with σ_r value set only from the minor axis objects and σ_ϕ value set only from the major axis objects. Therefore, we are able to obtain the values of the dispersion velocity per component only by fitting σ_{los} as a free parameter in the MLE. Moreover, for a cold system with a flat rotation curve as expected from the disc of S0 galaxies, we can also apply the epicyclic approximation:

$\sigma_\phi/\sigma_r = 1/\sqrt{2}$ (Binney and Tremaine, 1987). Therefore, we obtain information from σ_{los} in both radial and azimuthal directions without complicating the MLE method with too many free parameters.

The probabilities f_i obtained from the *f-map* in section 3.3 are used on eq. 3.9 to add the photometric information previously obtained into the final probabilities from the kinematics. They are divided by the velocity dispersion of each component to ensure the normalisation of the distribution.

Finally, using this model, C13b obtained the V, σ_{sph}, σ_r and σ_ϕ parameters for the velocity distribution of PNe of our sample galaxies, in elliptical bins along each galaxy radius and MLE. In the present work, we proceed by using eq. 3.9 with these estimated parameters to calculate, for our samples of spectroscopic GCs, their probabilities of belonging to the spheroid and disc components of each galaxy. In C16, this same procedure was adopted for the GCs of NGC 1023. Moreover, adopting this time a *likelihood clipping threshold* of 2.3σ, we can potentially detect GCs that are not compatible with the velocity distribution function from equation 3.9. If such kind of GC is present in a given galaxy, it can be considered an object in loose agreement with the galaxy overall kinematics and therefore potential merger remnant or interacting systems far from kinematical equilibrium with the studied galaxy gravitational potential.

3.7 Chromodynamical Analysis

Now that we have calculated the best-fit mean rotational velocity for the GCs, V, their dispersion velocity σ and the probabilities to belong to each component of the host galaxy considering the galaxy's velocity distribution function obtained from PNe in C13b, we can analyse this data from several perspectives. One that holds particular interest is the analysis of how the colour subpopulations of GCs behave in what regards the probabilities of belonging to the spheroid and the disc of its host galaxy. Also, it is of great importance to analyse the possible GCs that are not compatible with the velocity distribution obtained from PNe, since this can point

towards on-going mergers or interactions. In the next section we present the results from the application of the methods described in this chapter to our galaxy sample and their associated GCs and PNe.

Chapter 4

Results and Discussion

In this chapter we discuss the results obtained with the methods described previously (Chapter 3). We focus on the rotation curves derived from GCs obtained with the Maximum Likelihood Fit developed in C11, and analyse the results within formation scenarios proposed by simulations and observations from the literature. Additionally, we present several other properties of our sample galaxies that can be studied with the information of the kinematic and photometric likelihoods of a given GC to belong to the disc or the spheroid of the host galaxy. We show that our studied galaxies have very distinct GC kinematic properties, which is evidence for how diverse and complex the formation of S0 galaxies can be.

4.1 Rotation Curves derived from GCs and PNe

In fig 4.1 we present the results of the likelihood analysis described in the last chapter. In addition to the rotation curves obtained from the MLE fit for GCs using eq. 3.8, we present the same quantities for PNe adopting a single component model with only disc kinematics. For NGC 3115 and NGC 7457, these PNe fits are from C13a. For NGC 2768, the PNe single-component fit was obtained from Forbes et al. (2012). The idea is to compare both kinematic tracers in a single component fit, and once again considering PNe as tracers of the host galaxy kinematics (Napolitano et al., 2001; Coccato et al., 2009; Cortesi et al., 2011).

For NGC 3115 and NGC 7457, all the GC colour subpopulations rotation curves and dispersion velocity profiles show good agreement with the same quantities calculated for PNe at all radii. For NGC 2768, however, there is no clear accordance between GC and PNe kinematics, with only a slight agreement between red GCs and PNe. Also, NGC 3115 GCs and NGC 2768 red GCs show very distinct rotation curves. NGC 7457 has a smaller GC sample than the other galaxies in this work. Nevertheless, the robustness of the method enables us to compare consistently GCs and PNe. For comparison purposes, we have also added absorption lines, faint-fuzzies, GCs and PNe rotation curves for NGC 1023 that have been published in C16. Notice how the the rotation curve derived solely from GCs and PNe for NGC 1023 shows a decrease in rotation at large radii in the same way as the GCs and PNe of NGC 3115.

As far as the rotational velocity is concerned, our studied sample of galaxies have very distinct profiles: NGC 2768 has strong kinematic discrepancies between its GC colour subpopulations, with red GCs having a subtle increase in rotation velocity with radii and blue GCs rotational velocity showing an opposite behaviour. Interestingly, the PNe rotational velocity for this galaxy do not seem to be compatible with none of the GC colour subpopulations, considering the one-component kinematic model. The rotational velocity of NGC 3115 decreases with radius consistently for both GC colour subpopulations, in a similar way as NGC 1023, the blue GCs of NGC 2768 and NGC 3115 PNe. Lastly, NGC 7457 GCs have increasing velocities with radii, again in accordance with its PNe.

For the dispersion velocity, all galaxies show good agreement between PNe and GCs, even in the cases where the rotational velocities between these two tracers were not found to be compatible. For NGC 3115 and NGC 7457, the values for dispersion velocity are lower than the rotational velocity of GCs, except for the last two bins of NGC 3115 red GCs. The blue GC population of NGC 2768 after about 300 arcsecs (or 29.3 Kpc) do not show rotation anymore but we are still able to find a value of dispersion velocity somewhat constant with radius. The red GCs of NGC 2768 show very similar values for dispersion velocities and rotational velocities, while this is not true for the PNe in this galaxy.

Moreover, the likelihood fit also offers us the advantage of detecting objects that are

not kinematically compatible with the kinematics of the host galaxy, as shown in sec. 3.5. Such objects account for 10 GCs in NGC 2768, 32 GCs in NGC 3115 and 4 GCs in NGC 7457. This means that 21.5% of NGC 3115 GCs are not compatible with the galaxy kinematics. A higher amount than the 9.4% rejected objects in NGC 2768 and 10% in NGC 7457.

4.2 Comparison of GC and PNe kinematics

In order to understand how similar the GC kinematics is from the PNe kinematics, we present, in fig 4.2, the comparison of the GC kinematics with the PNe kinematics from the likelihood fits published in C13b. The PNe fits this time assume a two-component model, both spheroid and disc kinematics. PNe are excellent tracers of their host galaxy stellar population (Napolitano et al., 2001; Coccato et al., 2009). Therefore, this comparison has the potential to tell us how well GCs can be used to trace the host galaxy population in general. For the PNe of NGC 2768, the fit was allowed to calculate the rotation in both spheroid and disc components. For the other two galaxies, PNe only show rotation in the disc.

For NGC 2768 we can see that the GC rotation curve agrees better, within the errors, with the PNe rotation curve for the spheroid, when compared to the PNe rotation curve for the disc. NGC 3115 also does not show agreement between GC rotation curves and the PNe rotation curves of the disc. For NGC 7457, however, this agreement in the disc rotation is very clear. The highly disc-like kinematics of the GCs in this galaxy is a very distinct feature from the rest of the sample.

In fig. 4.2, PNe were fitted for a model with spheroid and disc dispersion velocities. Analysing how GC dispersion profiles compare with these quantities derived from PNe, we see a slight agreement between the dispersion velocity of PNe in the spheroid, σ_{sph} and GC dispersion velocities. We note that due to the low amount of points it is difficult to precisely define the statistical significance of any correlation between dispersion velocity profiles of GCs and PNe in this analysis, therefore we assume the results from this section as qualitative evidence.

To summarise, fig. 4.2 suggests that GCs of NGC 2768 and NGC 3115 do not trace

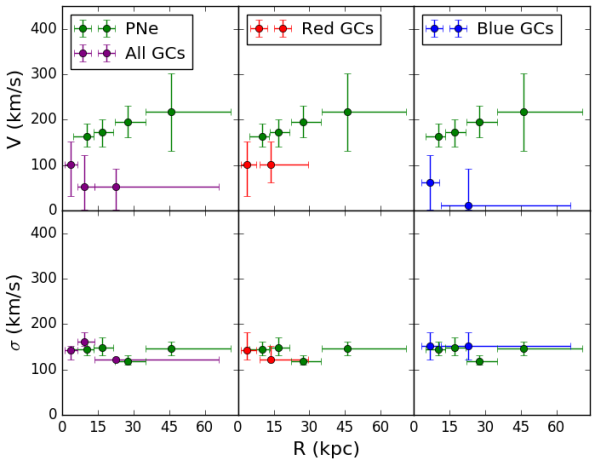

(a) NGC 2768

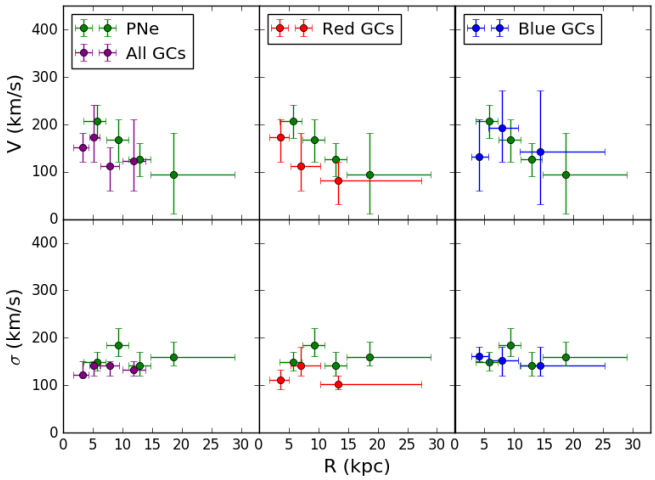

(b) NGC 3115

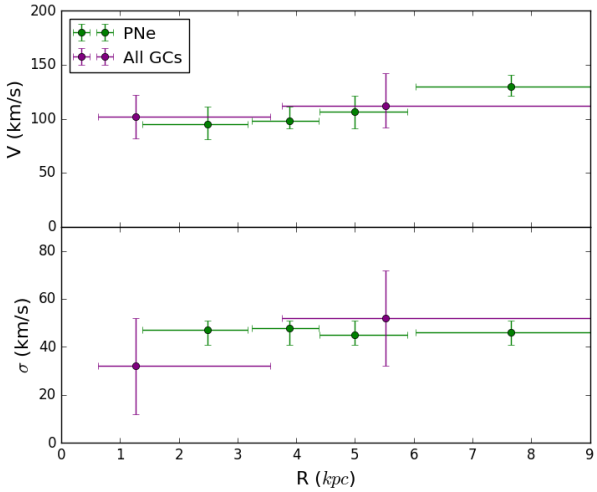

(c) NGC 7457

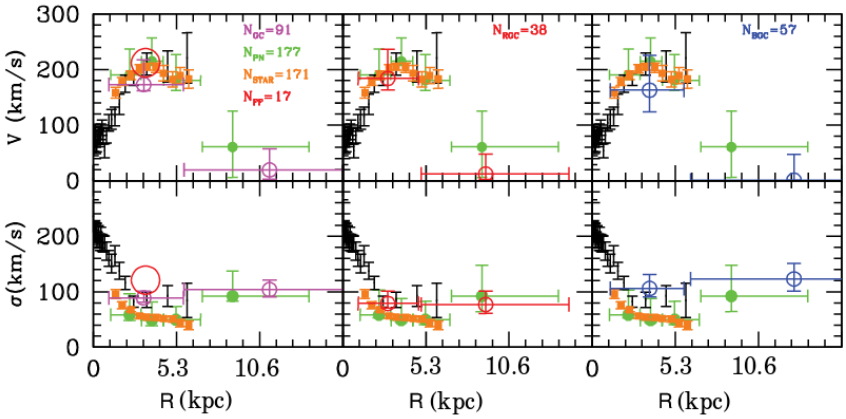

(d) NGC 1023, Cortesi et al. (2016)

Figure 4.1: Rotation curves and velocity dispersion for GC and PNe (from C13b) for our sample galaxies following the likelihood analysis. Vertical errorbars are the uncertainties and horizontal errobars represent binsizes. The data for NGC 1023 is adapted from C16, where green circles represent PNe data, black points are absorption line data (Debattista et al., 2002), orange circles represent stellar data obtained in Arnold et al. (2014) and the large red open circle represent faint-fuzzies from Larsen and Brodie (2000).

Table 4.1: Results of the likelihood analysis following photometry and kinematics for GC subpopulations.

Galaxies	Disc			Spheroid		
	Red GCs	Blue GCs	Total	Red GCs	Blue GCs	Total
NGC 2768	12	6	18	45	42	87
NGC 3115	40	36	76	41	32	73
NGC 7457	-	-	34	-	-	6

well the disc component of its host galaxy, but show promising results as tracers of spheroid kinematics. For NGC 7457, interestingly however, it is suggested a case of GCs that are able to trace disc kinematics of its host galaxy.

4.3 Colour and Kinematics

Having now the complete overview of the GC population of our sample galaxies using estimated kinematics and photometry within our model, we can analyse how the different subpopulations of GCs appear within the galaxies' components. For the red GC population of NGC 2768, 12 objects show a high probability of belonging to the disc while 45 show a high probability of belonging to the spheroid. In the blue GC population of NGC 2768, 6 objects show high probability of belonging to the disc, while 42 show a high probability of being present in the spheroid. For the red GC population of NGC 3115, 40 objects have a high probability of belonging to the disc while 41 have a higher probability of belonging to the spheroid. For blue GCs of NGC 3115, 36 objects are likely to be from the disc while 32 objects are likely from the spheroid. For NGC 7457, 34 GCs show high probability of belonging to the disc and 6 are more likely to belong to the spheroid. These results are summarised in table 4.1.

NGC 2768 show the predicted behaviour of having its GC population with kinematics associated with the spheroidal component, for all colour subpopulations, but with a smaller number of GCs with high probabilities of belonging to the disc. On the other hand, interestingly, the GC population of NGC 7457 is predominantly associated with disc kinematics and NGC 3115 has a similar number of GCs with disc and spheroidal kinematics. Shapiro et al. (2010), proposed that the red subpopulation of GCs can be formed at a redshift of $z \approx 2$ in

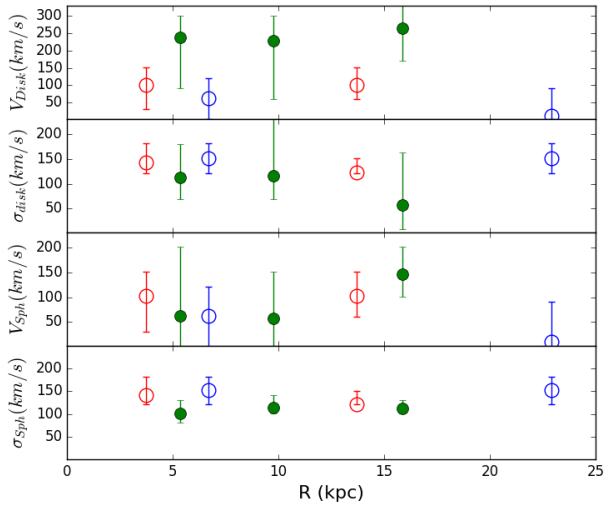

(a) NGC 2768

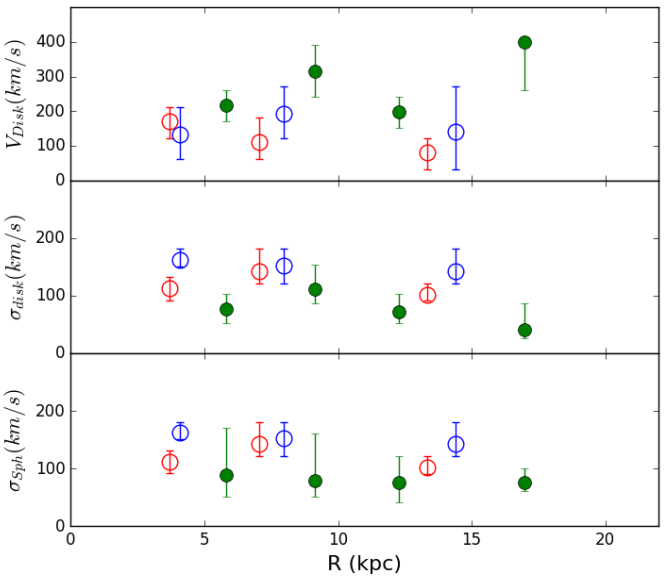

(b) NGC 3115

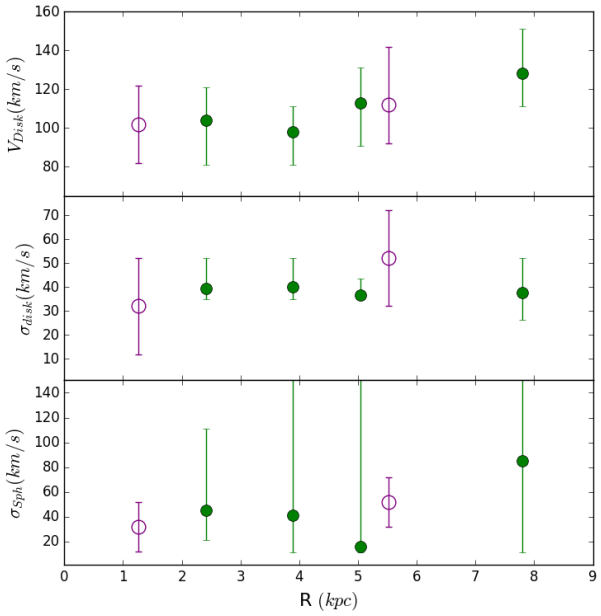

(c) NGC 7457

Figure 4.2: Comparison of the rotation curves and velocity dispersion obtained from GCs with the same quantities for PNe of our sample galaxies. Green filled circles represent PNe from C13b, where a two component kinematic fit was performed. Red circles represent the red GCs and blue circles represent the blue GCs. Magenta GCs represent the overall population of GCs. In all panels, the velocity and dispersion values for GCs are the V and σ values from fig. 4.1, respectively.

turbulent and violent disc formations. This would leave imprints of disc-like kinematics in GC populations, even if the disc does not survive to the present time. Therefore, the presence of GCs compatible with disc kinematics on all galaxies, but specially in NGC 3115 and NGC 7457, could be evidence of clumpy disc formation in such systems.

4.4 Final probabilities of belonging to the spheroid combining photometry and kinematics

We now present, in fig. 4.3, the recovered probabilities of our sample galaxies GCs to belong to the spheroid, now with the kinematic parameters obtained from the likelihood fit, i.e., the first term on the left side of eq. 3.9. As explained in section 3.6, the new probabilities also have the information of the PNe fit obtained in C13b for all galaxies. The most prominent feature noticeable is the drastic decrease of probability values around 0.5 from the photometry only histogram to the photometry and kinematic histogram. This shows the core improvement of the Maximum Likelihood Method over the photometric only approach. Projection effects severely reduce the ability to recover precise probabilities of component belonging based only on photometry, but are much less significant when kinematic information is added.

As such, we can clearly see that for NGC 2768, the GC population has a tendency to belong to the spheroid, with values of the probability to belong to the spheroid considering kinematics and photometry, L_{Sph}, close to 1. There is, nevertheless, a small amount of disc-like GCs in this galaxy. NGC 2768 has a more dominant spheroidal GC population than the other galaxies, a fact in accordance with the value of 0.7 for the bulge-to-total ratio of this galaxy (Forbes et al., 2012). NGC 3115 has an almost equal amount of disc and spheroid GCs, an unusual feature but also compatible with the prominent disc that observations of this galaxy seem to indicate (Guérou et al., 2016). NGC 7457 has an even more unusual higher amount of disc GC with very few objects with spheroidal kinematics. Chomiuk et al. (2008) and Hargis et al. (2011) have already found peculiar properties on the distribution of this galaxy GCs and stellar kinematics, which we will be further discussed in sec. 4.7.

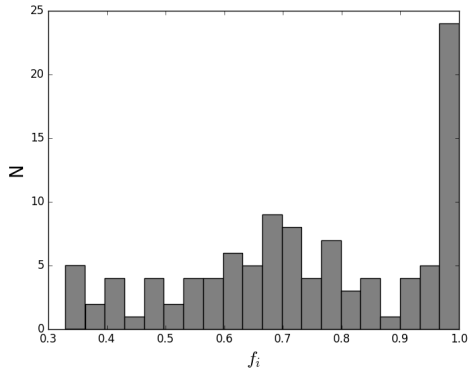

(a) NGC 2768 Photometry

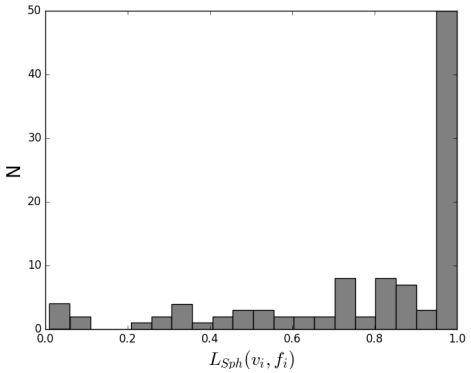

(b) NGC 2768 Photometry + Kinematics

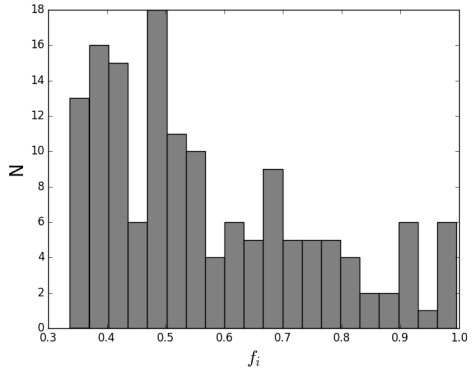

(c) NGC 3115 Photometry Only

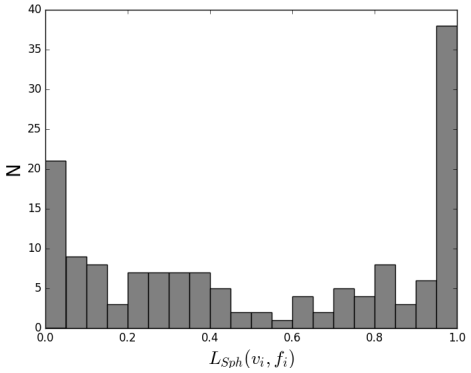

(d) NGC 3115 Photometry + Kinematics

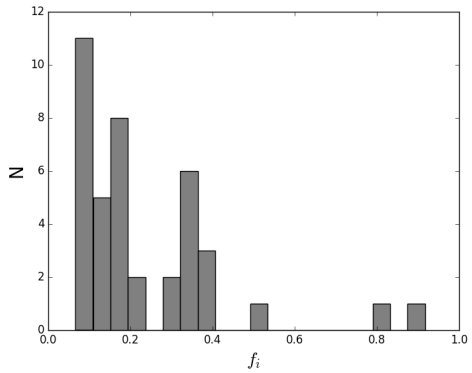

(e) NGC 7457 Photometry Only

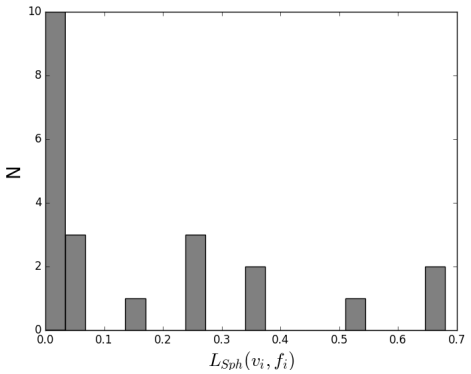

(f) NGC 7457 Photometry + Kinematics

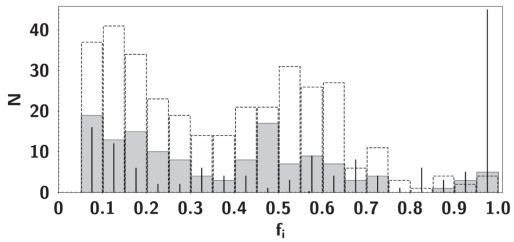

(g) NGC 1023 Photometry Only

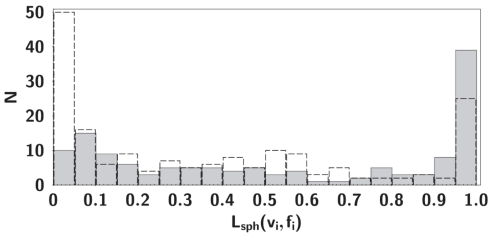

(h) NGC 1023 Photometry + Kinematics

Figure 4.3: The probability of GCs belonging to the spheroid.*Left panels*: results from photometry only analysis; *right panels*: results from photometry and kinematics after the likelihood fit. Notice the decrease of objects with probability values around 0.5 in the right panels compared to the left ones. In the bottom panels, we present this analysis for NGC 1023 from C16, where the filled bins represent GCs, open bins represent PNe information and the vertical lines comes from a random distribution of objects with a $1/r$ density fall-of.

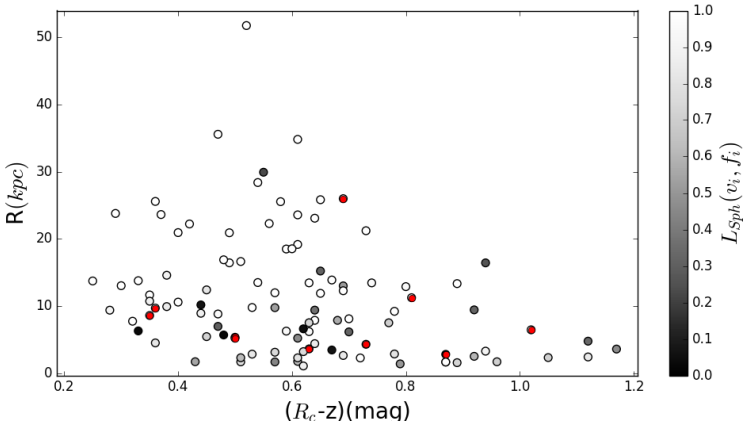

(a) NGC 2768

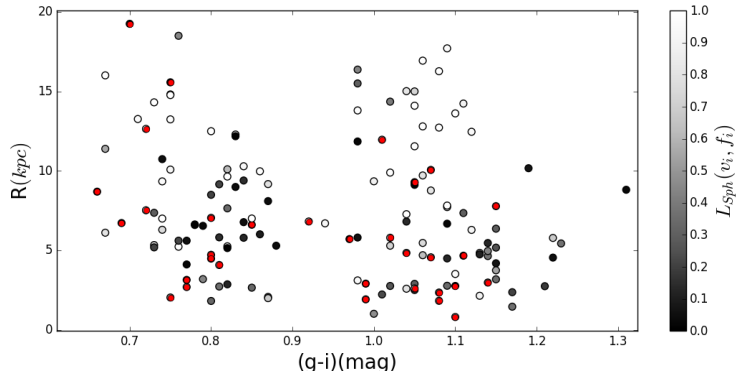

(b) NGC 3115

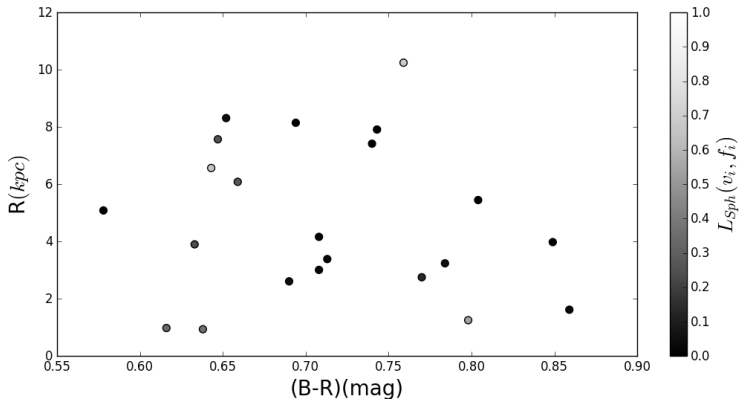

(c) NGC 7457

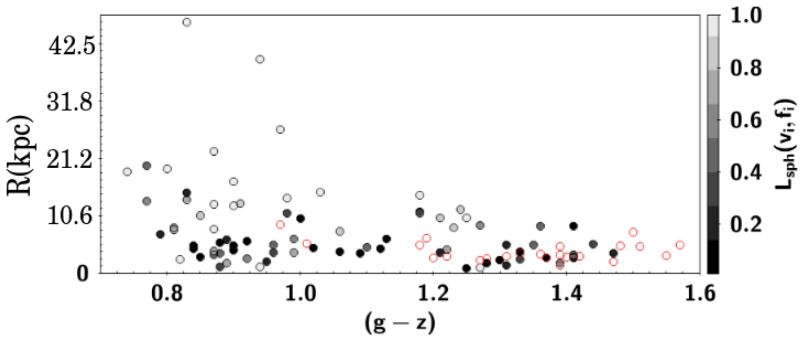

(d) NGC 1023, Cortesi et al. (2016)

Figure 4.4: Radial distribution of GCs colour coded by $L_{Sph}(v_i, f_i)$, the probability of belonging to the spheroid. Red filled circles represent rejected objects with kinematics not compatible with its host galaxy kinematics. NGC 1023 data is added for comparison, taken from C16, and in such case, open red circles represent Faint-Fuzzies.

4.5 Radial distribution analysis

We can now analyse how the radial distribution of GCs relates to their probability of being kinematic and photometrically related to the different host galaxy components. In fig 4.4 we show the radial distribution of GCs coded by the probability of belonging to the spheroid, $L_{Sph}(v_i, f_i)$. Note that disc GCs extend into large radii for all galaxies, at distances of at least $5R_e$. At first glance, the majority of objects with high probability of being in the disc are closer to the centre of the galaxy, as expected, for all objects. However, some outliers do exist, especially for the case of NGC 3115 (fig 4.4(b)). These objects are generally rejected in the likelihood fit and therefore have exotic kinematics compared to the host galaxy system.

No direct evidence of a correlation between colour and disc or spheroid likelihood can be seen for any of the sample galaxies. In NGC 3115, that shows a strongly bimodal GC colour distribution, for instance, there is almost equal amounts of disc-like and spheroid-like objects in each subpopulation. For NGC 2768, there is a slightly larger amount of spheroid GCs on the red population and closer to the centre of the galaxy, as found by Forbes et al. (2012).

Fig. 4.4 (c) shows 22 GCs from NGC 7457 that come from our spectroscopic sample of 40 GCs from Forbes et al. (2017). We lack photometry data for 18 objects in the spectroscopy sample, since we rely on public available data. This, however, should be of minimal importance since there is no signs of bimodality in this galaxy. Also, included in the 18 objects with missing photometry are the rejected objects by the likelihood fit.

Moreover, one can analyse how GC colour subpopulations are related to both radial distribution and disc or spheroid belonging probabilities. We can clearly see that the colour bimodality stands much more obvious for NGC 3115 than for NGC 2768, but this doesn't relate directly to a clear pattern of disc-bulge belonging for those objects. Therefore, the bimodality in colour displayed for the GC subpopulations does not seem to follow up to a spatial distribution for GCs in such galaxies, at least when considering the disc and spheroid components. When considering that the spheroid modelled in this work comprises both halo and bulge components actually, the conclusion becomes less strong. In the Milky Way, for instance, blue and red

GCs are also less present in the disc but well divided between a halo, blue and metal-poor GC population and a bulge, red and metal-rich population (Larsen et al., 2001; Peng et al., 2006). Forbes et al. (2012) has already shown that the red GC subpopulation of NGC 2768 is more related to the bulge specifically. In summary, the bimodality in colour following up to a spatial bimodality is not to be completely discarded, yet, for the galaxies studied here.

Nevertheless, taking into consideration the aforementioned reasonable assumption that GCs should be more prevalent in the spheroid, it is interesting to note such a significant amount of disc GCs in all colour subpopulations. This could lead to interesting consequences on possible formation scenarios. Such issue will be discussed later on in this chapter after more information is added.

4.6 Phase-space diagrams

In addition to the radial distribution of the recovered probabilities of belonging to the host galaxies' spheroidal regions, it is interesting to analyse the phase-space diagrams for the GCs with the information from the recovered probabilities. Phase-space diagrams consist on the line-of-sight velocities of objects plotted versus the radial position of such object within the host galaxy. This diagram can shed light on how the overall kinematics of the galaxy is related to its spatial distribution (Rocha et al., 2012). In general, we expect a somewhat 'bell shaped' pattern for such phase-space diagrams, since objects closer to centre of a given galaxy should display more rotation, and therefore a more scattered distribution (Strader et al., 2011). When we go far into the galactic halo, objects are expected to rotate much less and display hot kinematics. For this work, we decided to use instead of directly the line-of-sight velocities, the quantity $\Delta V = V_{los} - V_{sys}$, where V_{sys} is the systemic velocity of a given galaxy obtained from The NASA/IPAC Extragalactic Database (NED). In this way one can readily compare the 4 galaxies in this work. To emphasise even more the results of this section, we add PNe positions and velocities from Pota et al. (2013) that have been used in C13b to produce the rotation curves in Fig. 4.1. PNe are expected to trace strongly the disc kinematics (Napolitano et al., 2001;

Coccato et al., 2009), and therefore we generally expect not to find general agreement between GCs and PNe in the following diagrams, with the exception of NGC 3115 and NGC 7457 which show strong evidences of GCs compatible with the kinematics of the disc, as obtained previously.

Another useful property of phase-space diagrams is that they allow us to estimate the time an object started falling into its host galaxy gravitational potential, the infall time. Rocha et al. (2012) have shown that this is possible for the Milky Way by looking at how far an object is in a phase-space diagram from the host galaxy systemic velocity. In principle, objects with kinematics closer to the systemic velocity of the whole system are closer to kinematical equilibrium than objects that have been accreted by the galaxy and have *ex-situ* origins.

Fig. 4.5 shows the phase-space diagrams for our galaxies PNe and GC subpopulations. These GCs are separated both by colour and likelihood to belong to the spheroid or disc. Notice how in NGC 2768, fig. 4.5 (a), the blue population of GCs extends further out than the red GC population, although as seen in fig 4.4, both subpopulations show high probabilities of belonging to the spheroid. In fact, Forbes et al. (2012) when studying this galaxy kinematics specifically looking into its red GC population found that it is related to the kinematics of the stellar bulge of the galaxy. Therefore, it is reasonable to say that as the blue GC population in this galaxy have a high probability of being in the spheroid and is not radially correlated with the red GCs, it should be located predominantly in the halo. No correlation can be clearly seen between colour and infall time for this galaxy GCs, although it is interesting to note that farther away from the center of NGC 2768, objects seem to be more in equilibrium with its kinematics than at close radii. This indicates that such objects can have *in-situ* origins, while *ex-situ* objects were somehow brought into the host galaxy inner regions after accretion.

In the phase-space diagram for GCs and PNe of NGC 3115, fig. 4.5 (b), one can see that GCs with high probabilities to belong to the disc are located on the edge of the distribution, even at large radii. This indicates, as aforementioned, objects that display rotation. Notice the symmetry of the location of disc-like GCs in the diagram and the consistency of this pattern even at large radii (up to 18 Kpc). Rejected objects from the likelihood analysis also display a

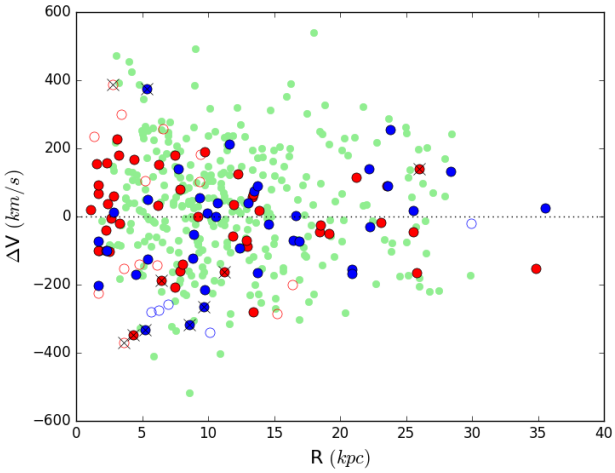

(a) NGC 2768

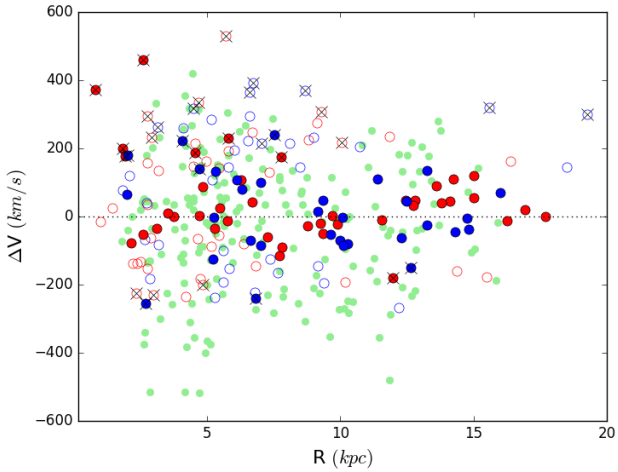

(b) NGC 3115

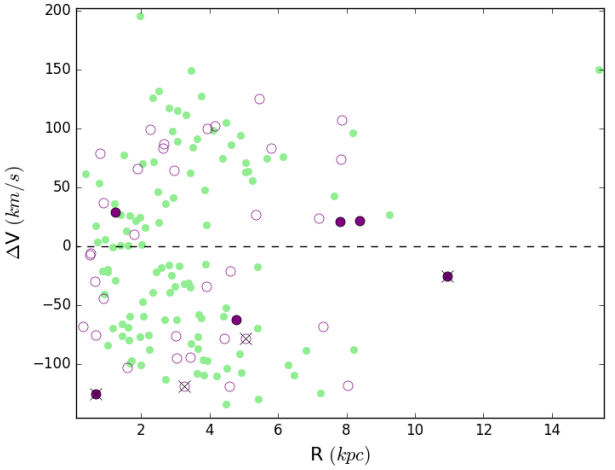

(c) NGC 7457

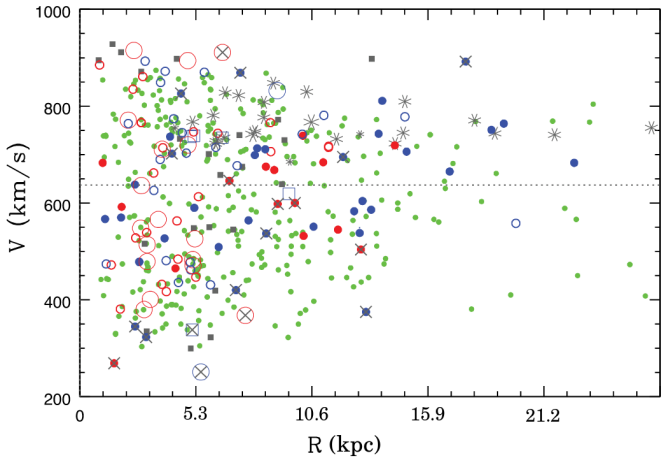

(d) NGC 1023

Figure 4.5: Phase-space diagrams for GCs and PNe. Objects likely to belong to the spheroid are represented by filled circles, and objects with high probability of being part of the disc are represented by open circles. Blue and red GCs are represented by their respective colours. Green filled circles are PNe. For NGC 7457, due to its lack of bimodality in colour, we show only disc and spheroid populations. Objects marked with crosses are rejections from the kinematic fit. On the bottom-right, we show the phase-space diagram for NGC 1023 published in C16. For this plot, rejected objects are shown as crosses (GCs), squares (PNe and stars) and stars (objects associated with the companion galaxy NGC 1023A).

rather interesting distribution in the diagram. Most of them have similar values of ΔV, around 200 Km/s larger than the host galaxy systemic velocity. Such fact indicates that these GCs may form a coherent structure from *ex-situ* origin that recently was accreted by this galaxy, or remnants of a minor merger that still remain scattered at different radii with imprints of their original kinematics.

For NGC 7457, by analysing fig. 4.5 (c), we see a more compact distribution of GCs and PNe in the phase-space diagram, with objects showing values of ΔV of $\leq$ 200 km/s. NGC 2768 and NGC 3115 have GCs with values of ΔV in the range of 600 km/s, therefore, NGC 7457 is a system, at least in principle, in a more developed kinematic equilibrium than the other galaxies in our sample. The small amount of rejected objects from the likelihood fit for this galaxy corroborates with this hypothesis. The high amount of GCs with high probabilities to belong to the disc of this galaxy have similar loci on the phase-space diagram as the PNe, and show an 'U' shaped distribution. This shape is due to the higher amount of rotation displayed by the GCs and PNe of this galaxy. Only at small radii, at around 2 kpc or less, this galaxy shows GCs and PNe with values of ΔV close to zero. In summary, NGC 7457 seems to be a very rotationally supported galaxy.

In addition to fig. 4.5, it is interesting to analyse the distribution of the velocities of the tracers versus the distance projected onto the major axis of host galaxies. This complements the phase-space analysis and is useful to pinpoint possible ongoing interactions. For the case of NGC 3115, for instance, judging by fig 4.5 (b), although the colour bimodality for this galaxy's GCs is very strong, kinematically both subpopulations do not differ significantly. The GCs that are not kinematically in equilibrium with the galaxy kinematic model used on the likelihood fit, on the other hand, show interesting properties. They seem to be early accreted objects, judging by the suggested infall times from the phase-space diagram, and seem to form a connected structure. In fig. 4.6 they are also present in a somewhat connected structure, albeit fairly large.

Chies-Santos et al. (2013) analysed a ΔV versus distance along the major axis diagram for the PNe of NGC 1023. Later, C16 published this same diagram for NGC 1023 adding

GCs and stellar absorption line data. We present, for comparison purposes, in fig. 4.5(d) and fig. 4.6 (d) the phase space diagram and ΔV versus distance along the major axis for GCs, PNe and stellar absorption lines of NGC 1023 published in C16. For this galaxy, objects rejected from the kinematic fit, represented by asterisks, are very concentrated and seem to be related to the companion galaxy, NGC 1023A. NGC 3115 rejected GCs form a less concentrated structure and therefore would be more compatible with being remnants of a recent merger than with companion galaxies.

Finally, NGC 7457 has a very disc-like shaped distribution in fig. 4.6 both for PNe and GCs, as expected from the analysis of the rotation curves. All objects seem to be in a reasonable equilibrium with the galaxy's kinematic system, showing evidence of it being a relaxed system. If violent episodes occurred in this galaxy's past, they were not recent enough to still leave imprints in the galaxy's dynamics. This argument is compatible with the hypothesis of a clumpy disc formation producing this large GC population with disc-like kinematics.

In an interesting consideration, both fig. 4.5 and fig. 4.6 combine information previously known from observations of the individual objects velocities with the probabilities obtained in this work from both photometry, kinematics and the likelihood fit. The results from this section show that the posteriori results agree very well with our observational basis, a confirmation of the reliability of the maximum likelihood method developed in C16 and used here.

4.7 V/σ ratio and discussion

In this section, we will analyse the GC rotation curves and the V/σ ratio for all GC populations of sample galaxies to compare our results with simulations from the literature. The V/σ quantity is used as an indicator of how much the kinematics of a galaxy is influenced by rotational velocity, in the case of higher values, or is more influenced by random motions, in the case of a ratio smaller than 1. The GC rotation curves are in general, not necessarily similar with the general kinematics of a galaxy, and, most often than not, are not completely

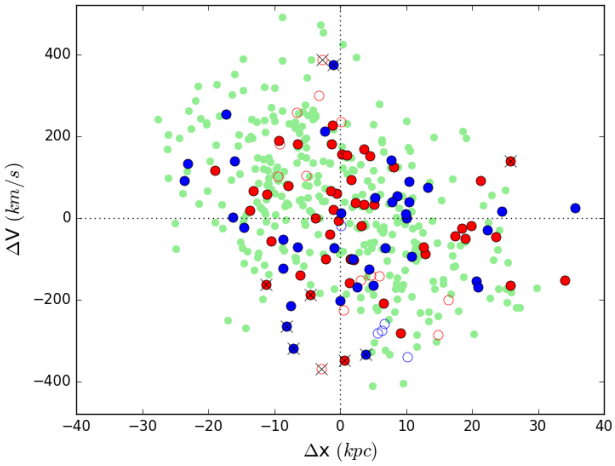

(a) NGC 2768

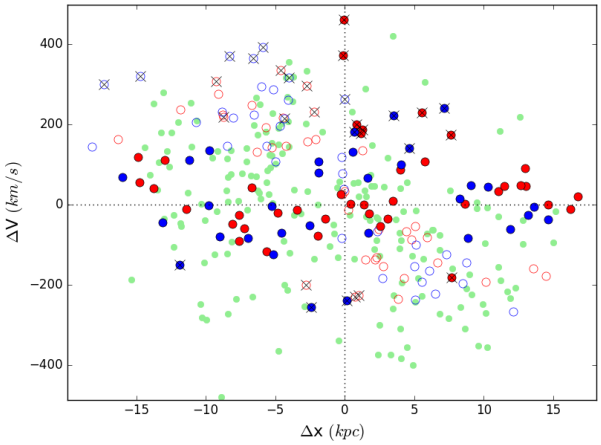

(b) NGC 3115

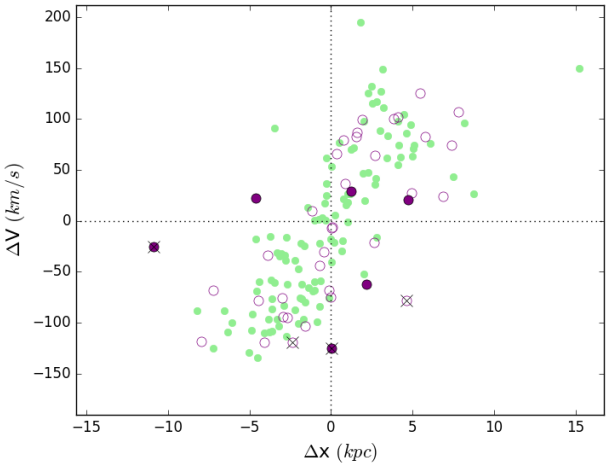

(c) NGC 7457

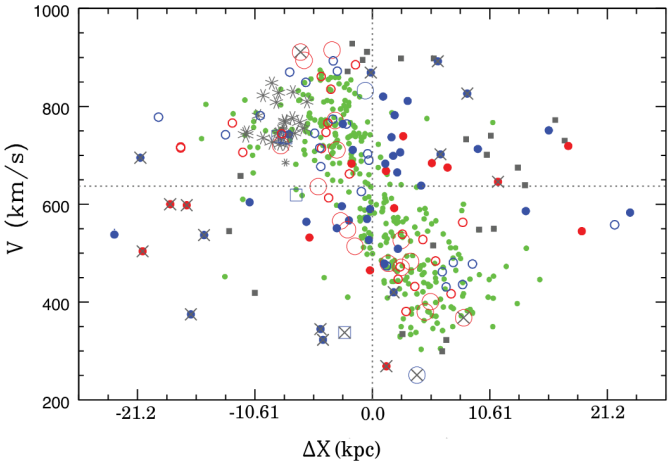

(d) NGC 1023

Figure 4.6: Velocity versus distance along the major axis for GCs and PNe of our sample galaxies and NGC 1023 published on C16. Markers are the same as in fig. 4.5 for all panels.

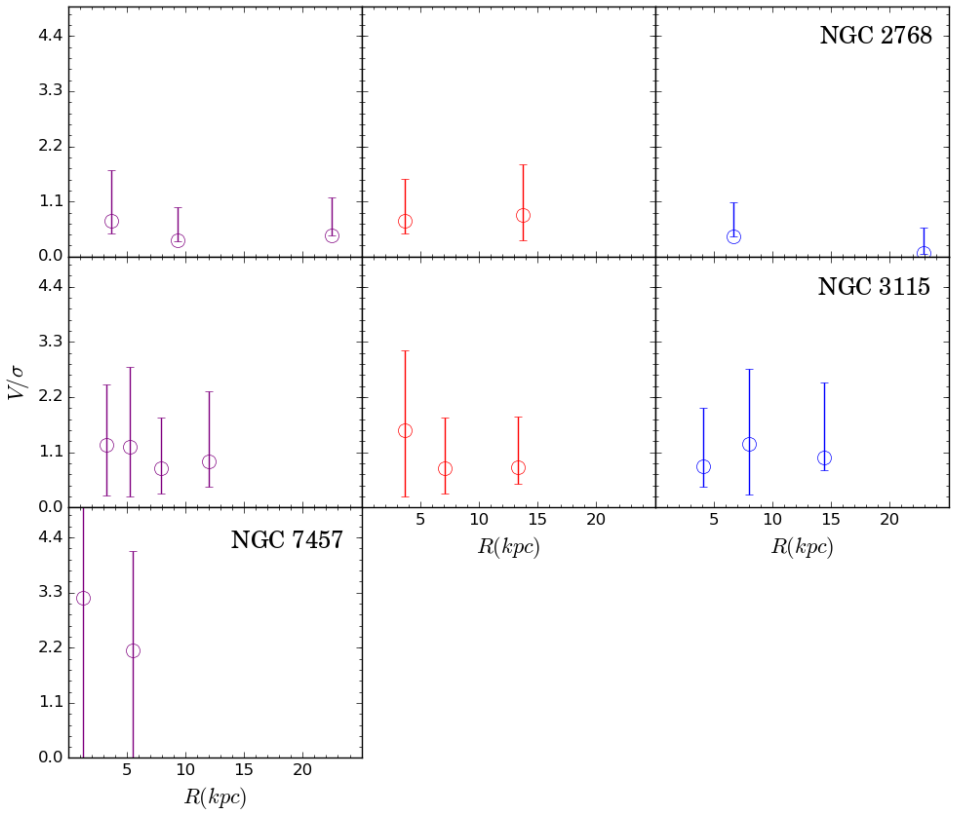

Figure 4.7: V/σ ratio for our sample galaxies obtained from GCs. *Left*, full sample of GCs for each galaxy, *centre*: Red subpopulation of GCs, *right*: blue subpopulation of GCs. NGC 7457 has no signs of significant bimodality so only one population is shown. The errorbars for NGC 7457 GCs are in the order of $\delta V/\sigma \approx \pm 3.0$.

in dynamical equilibrium with the host galaxy kinematics. This is specially true when the evolution of a galaxy revolves around mergers, that can bring *ex-situ* objects into the progenitor kinematic system. Nevertheless, GC kinematics can be used as great tools when tracing back the evolution of galaxies.

Bekki et al. (2005), studied with dissipationless numerical simulations the outcome of various mergers scenarios on the GC kinematics of early-type galaxies. They showed that mergers with a proportion of 10:1 are able to produce flattened early-type galaxies such as lenticulars and should impact the kinematics of GCs in such a way that the rotation at large radii of the GC system would be smaller than at closer radii. Bournaud et al. (2005) showed that minor mergers with a proportion of 4.5:1 would produce a $v/\sigma \approx 1$ on the remaining galaxy and a merger with a proportion of 10:1, such as the ones Bekki et al. (2005) studied, would produce a $v/\sigma \approx 2$. Besides a major merger event, another likely path on the evolution of galaxies in various environments is a sequence of minor mergers that could produce a faster consumption of the available gas in the initial galaxy, but not in a single episode. Moody et al. (2014) showed that multiple minor mergers would not produce, however, fast rotating galaxies (Emsellem et al., 2011), but instead being more likely to produce hot, elliptical and slow rotating galaxies.

In fig. 4.7 we show the V/σ ratios obtained from the GC subpopulations using the method described in the last chapter and the results from fig. 4.1. One can see that the values of v/σ for NGC 3115 are close to or smaller than 1 for GC subpopulations and for all radii, so that would corroborate with the proposition that this galaxy is a remnant of a merger with a proportion of, at least, 4.5:1. This merger would have been not strong enough to rip the disc structure of the galaxy apart, but significant enough to accelerate the gas removal in the galaxy. NGC 3115 also has a known prominent disc structure, with even signs of spiral arms (Norris et al., 2006; Guérou et al., 2016). This suggests that if this galaxy formed through a merger, then it was not strong enough to disrupt not even fragile structures such as spiral arms. Additionally, in most findings of our study shown in this work and C16, NGC 3115 and NGC 1023 show very similar GC kinematics. In C16, it was argued that for NGC 1023 the ratio between the rotation velocity and the velocity dispersion in the azimuthal direction is not

compatible with a faded spiral galaxy, but instead consistent with minor mergers. Therefore, the same seems to be the case for NGC 3115.

NGC 2768 shows a very different scenario than previous galaxies, presenting rotation at large radii for its red GCs and PNe population. This is evidence of two possible formation hypothesis: the outcome of the gas stripping of a regular spiral galaxy, or a merger scenario more closely related to what could produce elliptical galaxies. NGC 2768 does indeed has a more prominent spheroidal structure than the other galaxies in this sample, so a major merger with a proportion larger than 4.5:1 but still not strong enough to disrupt completely the disc structure of the progenitor galaxy is a possibility for the formation of such system. The v/σ ratio of this galaxy however shows similar values for all GC subpopulations when compared to NGC 3115, a galaxy with a prominent disc component. Forbes et al. (2012) argued that the radial distribution of the v/σ ratio of this galaxy is similar to late-type galaxies by studying its red GC population, PNe and starlight. This galaxy shows a complex pattern of kinematic properties, not easy to put into simple formation scenarios. Nevertheless, it is clear that this galaxy has had an evolution different from, at least, NGC 3115 and NGC 1023. This result shows how diverse and more complex than expected the formation of S0 galaxies turns out to be.

NGC 7457 is a particular case, since unlike the other galaxies in the sample, it has a dominant disc GC population from the results of the likelihood analysis. This galaxy has fewer GCs overall (around 210, from analysis of surface density profile in Hargis et al. (2011)), from which we have 40 spectroscopic GCs, and therefore a slightly less reliable likelihood fit. Nevertheless, the results from the GC rotation curve are well in agreement with the results for PNe published in Cortesi et al. (2013b) that had a sample larger by more than 100%. Hargis et al. (2011) studied the GC system of NGC 7457 and concluded that although the spatial distribution of the system is very elliptical, an inclined disc GC population could explain the properties found in his work. In the same work, it was suggested that the most likely formation scenario for this galaxy is through mergers. NGC 7457 is a field galaxy, so gas stripping mechanisms which usually are related to dense environments is a very complicated hypothesis to maintain. Also, additionally to the unusual distribution of the GCs in NGC

7457 components, the GC system apparent lack of bimodality in colour is rather difficult to accommodate into formation scenarios. Presently in the literature, most scenarios for early-type galaxy formation involve a two-phase of galaxy formation (Oser et al., 2010) in which the bimodality of GCs in colour, metallicity and age would be a more natural outcome. However, recently, Peacock et al. (2017) studied this galaxy and found a slightly more numerous GC sample than previous studies, such as Hargis et al. (2011) and Pota et al. (2013). This slightly larger sample show signs of bimodality in the $(g-z)$ colour, albeit small. The v/σ ratio for this galaxy is more than 2, which would mean, following Bournaud et al. (2005), a merger origin with a proportion of around 10:1, at most. Another piece of information that can be added into this puzzle comes from Alabi et al. (2017). In this work, the dark matter fraction at large radii for this galaxy was studied and found to revolve around 0.9 within 5 R_e. This is much greater than the dark matter fraction values found for NGC 2768, NGC 3115 and NGC 1023 in the same work, which are all around 0.6. With this information, Alabi et al. (2017) have calculated an assembly epoch for the halo of NGC 7457 at $z \approx 4.4 \pm 1.1$, or 12.3 Gyr ago. However, the mean luminosity-weighted age for the stellar content of the central regions of this galaxy and some of its GCs is around 3-7 Gyr (Sil'chenko et al., 2002; McDermid et al., 2015; Chomiuk et al., 2008). Therefore, the assembly of the halo of the galaxy took place long before the GCs and stars at the centre of the galaxy, compatible with a merger event in the galaxy past that triggered the formation of such objects. However, the simulations of Bekki et al. (2005) indicate that GC systems of galaxies that suffered minor mergers that would form flattened disc galaxies, such as NGC 7457, should retain a more spherical structure with little rotation at larger radii. In summary, this galaxy is a complicated object with clear evidences for a merger origin due to its isolation and kinematic properties, but lacking observed GCs in its outer regions to help explain this hypothesis. Undoubtedly this is a very interesting object to be studied further with a larger sample of spectroscopic GCs.

Chapter 5

Conclusion

In this dissertation we have presented the analysis of the kinematics of discrete tracers, GCs and PNe, for a sample of S0 galaxies. We have also obtained rotational velocities and dispersion profiles for GCs using a method presented in C16 that relies on a photometric spheroid-disc decomposition of galaxy images using GALFIT and a maximum likelihood estimation (MLE) to find the best fit kinematic parameters. We have also obtained the probabilities of our sample of spectroscopic GCs to belong to the spheroid and disc components of their host galaxies, using the velocity distribution for the entirety of such galaxies obtained with MLE using PNe from C13b. As an initial result, we have compared the GC radial density for our sample galaxies with surface brightness profiles obtained with GALFIT, finding generally a good agreement within errors for all galaxies. Additionally we found good agreement when comparing the kinematics of GCs with the kinematics of PNe when assuming for both tracers the same kinematic model in the MLE, for all galaxies in our sample, except for the case of NGC 2768. For this individual galaxy none of its GCs subpopulations have compatible kinematic profiles with PNe while also displaying a different kinematic behaviour between themselves. NGC 2768 presents evidences, therefore, of a more complex structure than what we see in the other galaxies, possibly implying a different formation mechanism for both its GC subpopulations. For the other galaxies our results suggest that GCs can be used efficiently to trace the kinematics of the spheroidal component of their host galaxies, comprising bulge and

halo, and even the disc kinematics on galaxies such as NGC 3115 and NGC 7457 that show a high number of GCs with kinematics compatible with the disc. Such results demonstrate that the method used in this study is a powerful tool to study the global kinematics of galaxies even at large radii, while conventional techniques employed for late-type galaxies are not as efficient in gas-poor galaxies such as lenticulars, or in their outskirts where stellar light is too faint.

In broad terms, our goal, however, was to use the kinematic information recovered to study the evolution of S0 galaxies. Proposed scenarios in the literature for the formation of such type of galaxies include: environmental processes such as ram-pressure stripping, starvation or harassment (Gunn and Gott, 1972; Dressler, 1980; McCarthy et al., 2008) and minor mergers, as a single event triggering the transformation of regular spiral galaxies or a series of interactions altering the original galaxy morphology into what we see today (Bournaud et al., 2005; Bekki et al., 2005; Oser et al., 2010). All of these scenarios start with typical spiral galaxies somehow losing their gas content and therefore halting their star formation rate but without having their disc structure completely disrupted as it would be the case in major merger events that are suggested to form elliptical galaxies (Bekki et al., 2005; Conselice, 2014).

The galaxies in our sample, NGC 2768, NGC 3115 and NGC 7457, with the addition of NGC 1023, previously studied with the same method in C16, are not located in high density environments, therefore we did not expect from the start to find evidence of ram-pressure stripping or similar processes associated with high density environments. Therefore, minor mergers would be more likely to explain the formation of such galaxies located in the field or in low density groups. The differences in the kinematics of GC subpopulations seen among them, however, showcase a heterogeneous scenario for these galaxies evolution.

5.1 Summary of Dissertation Achievements

After the discussion of the results presented in the last chapter, we reach the following conclusions for our individual galaxies:

- **NGC 2768** This galaxy GC colour subpopulations are found to be kinematically distinct, with its red GCs displaying an increase in rotational velocity with radii alongside a decrease in dispersion velocity for the same radial range, while its blue GCs show a decrease in rotational velocity with radius and almost constant values for their velocity dispersion. Forbes et al. (2012) found similar results in a study focused only on the red GCs of this galaxy, and proposed that this subpopulation of GCs are compatible with the kinematics of stars and PNe in the bulge component of the galaxy. The v/σ values for both of our colour subpopulations of GCs in this galaxy are, however, very similar for all radii, with values around 1. This is compatible with a merger origin with a proportion of at least 4.5:1 (Bournaud et al., 2005). In such merger scenario, however, we would expect to find rotation at large radii in this GC system (Bekki et al., 2005). While the red GCs have an increase in velocity radially, they do not extend as far as the blue GCs, which have negligible rotation at large radii. Thus we conclude that while a merger origin seems still more likely for this galaxy due to its overall kinematics, it might have experienced more than one event in its past that affected each of its GC subpopulations differently. Interestingly, we find only a few GCs with kinematics not compatible with the overall galaxy kinematics, making less probable that some GCs in this galaxy have recent *ex-situ* origins, which could explain the distinct kinematics.

- **NGC 3115** The PNe and GCs of this galaxy show very similar kinematics at all radii, with both red and blue GCs behaving very similarly between themselves as well. The rotational velocity in this galaxy decreases with radii with somewhat constant values for dispersion velocity. The values of v/σ remain close to 1 at all radii, suggesting again a merger origin of at least a 4.5:1 proportion (Bournaud et al., 2005). The high amount of disc compatible GCs and the remnants of spiral structures recently found in this galaxy (Guérou et al., 2016) suggest a very prominent and undisturbed disc structure. The ratio of rotational and dispersion velocities, however, is still lower than what would be expected for regular spiral galaxies. Moreover, this galaxy has around 20% of its GCs with kinematics not compatible with the overall stellar kinematics. Taking into account, all of these results suggest not a single merger event transforming an original spiral galaxy,

but several minor mergers that were sufficient to cause the galaxy to run out of gas but not violent enough to disrupt the disc. At least one of such events might have happened recently to explain the amount of GCs with low probabilities to belong to the galaxy based on kinematics. Finally, the kinematics of GCs and PNe share many similarities with the previously studied NGC 1023, which also was proposed to be formed through gentle mergers and is currently accreting a companion galaxy (C16).

- **NGC 7457** The GCs of this galaxy were found in this work to be predominantly related to the disc component of the galaxy, with few objects likely to belong to the spheroid. This galaxy has a relatively low amount of detected GCs (Hargis et al., 2011) and consequently our GC sample is much smaller than what we had for the other galaxies in our sample. Nevertheless, we found good agreement between the kinematics of this galaxy's GCs and PNe. There is a slight increase in rotation velocity with radius, but with values of the ratio v/σ around 2, larger than for the other galaxies in this sample. Initially, this points towards a merger origin with a proportion of 10:1 (Bournaud et al., 2005), therefore relatively subtle, enough to leave the kinematics of this galaxy disc highly undisturbed when compared to its past as a spiral galaxy. This is compatible with the fact that this galaxy is the most isolated of our sample, and therefore, less likely, in principle at least, to experience violent interactions with other galaxies with similar size. However, it is still puzzling to find so few GCs at large radii, even considering the photometric sample. The peculiar kinematic properties of this galaxy GCs and stars have been suggest as evidence of mergers (Chomiuk et al., 2008; Hargis et al., 2011), but the simulations of Bekki et al. (2005) indicate that if this was the case, its GCs should display hotter kinematics than what we have found. Also, Hargis et al. (2011) argues that even if the colour bimodality is not easily found for this GC system, it has a very similar colour distribution to the GC system of the Milky Way. A larger GC spectroscopic sample, therefore, would be of great help to understand the puzzling formation of this galaxy.

In summary, this work shows that the structure and kinematics of lenticular galaxies is very diverse and more complex than expected by most scenarios proposed in the literature.

Although mergers and environmental effects still stand as the most probable origins for such types of galaxies, their evolution seems to comprise several events that slowly transform regular disc galaxies into S0s, instead of few significant events.

5.2 Future Work

This work employed a method first presented in C16 to three S0 galaxies that complement the galaxy NGC 1023 studied with the method in C16. The MLE method showed once more its effectiveness in using discrete tracers to study the kinematics of such galaxies. As we found that each galaxy individually was more complex than expected, to study even more lenticular galaxies would be the first step to further enhance and solidify the evolution scenarios suggested by the results presented here. There are already strong candidates for galaxies to be studied in the future, such as NGC 5866 and NGC 0821, for which the spectroscopy of GCs was recently made available Forbes et al. (2017). For NGC 5866, a PNe analysis such as performed for our sample galaxies in C13b is currently in preparation. If larger spectroscopic samples of GCs and PNe are obtained for such galaxies in the future, it would also be interesting to revisit the results found here with a larger sample.

The study of other types of galaxy morphologies is also possible with the method presented here, especially other types of *early-type* galaxies, such as ellipticals. This could reveal possible similarities between their GC systems and the ones of lenticulars and spirals already studied in the literature, improving our understanding of the evolution and relations of galaxies of different morphologies.

Finally, the kinematic model that was used for the MLE can also be improved, possibly including additional galaxy components, such as separating the bulge and the halo, or thin and thick discs. This is already possible currently but naturally increases the amount of free parameters to be estimated in the MLE and therefore lowers the accuracy of the estimation and increases the computational resources needed. With the optimisation of the method and the codes used in this work, however, this could be made easier and would be very interesting

to disentangle the properties of galaxies that have structures apparently more complex than what we model here.

Bibliography

Alabi, A. B., Forbes, D. A., Romanowsky, A. J., Brodie, J. P., Strader, J., Janz, J., Usher, C., Spitler, L. R., Bellstedt, S., and Ferré-Mateu, A. (2017). The SLUGGS survey: dark matter fractions at large radii and assembly epochs of early-type galaxies from globular cluster kinematics. *Monthy Notices of the Royal Astronomical Society*, 468:3949–3964.

Arnold, J. A., Romanowsky, A. J., Brodie, J. P., Forbes, D. A., Strader, J., Spitler, L. R., Foster, C., Blom, C., Kartha, S. S., Pastorello, N., Pota, V., Usher, C., and Woodley, K. A. (2014). The SLUGGS Survey: Wide-field Stellar Kinematics of Early-type Galaxies. *Astrophysical Journal*, 791:80.

Ashman, K. M., Bird, C. M., and Zepf, S. E. (1994). Detecting bimodality in astronomical datasets. *Astronomical Journal*, 108:2348–2361.

Baba, H., Yasuda, N., Ichikawa, S.-I., Yagi, M., Iwamoto, N., Takata, T., Horaguchi, T., Taga, M., Watanabe, M., Okumura, S.-I., Ozawa, T., Yamamoto, N., and Hamabe, M. (2002). Development of public science archive system of Subaru Telescope. *Report of the National Astronomical Observatory of Japan*, 6:23–36.

Bekki, K., Beasley, M. A., Brodie, J. P., and Forbes, D. A. (2005). Kinematics of globular cluster systems and the formation of early-type galaxies. *Monthy Notices of the Royal Astronomical Society*, 363:1211–1222.

Binney, J. and Tremaine, S. (1987). *Galactic dynamics*.

Blakeslee, J. P. (1997). Globular Clusters in Brightest Cluster Galaxies. In *American Astronomical Society Meeting Abstracts #190*, volume 29 of *Bulletin of the American Astronomical Society*, page 848.

Blakeslee, J. P., Cantiello, M., and Peng, E. W. (2010). The Mass-Metallicity Relation of Globular Clusters in the Context of Nonlinear Color-Metallicty Relations. *Astrophysical Journal*, 710:51–63.

Bournaud, F., Jog, C. J., and Combes, F. (2005). Galaxy mergers with various mass ratios: Properties of remnants. *Astronomy & Astrophysics*, 437:69–85.

Brodie, J. P. and Larsen, S. S. (2002). New Members of the Cluster Family in Nearby Lenticular Galaxies. *Astronomical Journal*, 124:1410–1417.

Brodie, J. P., Romanowsky, A. J., Strader, J., Forbes, D. A., Foster, C., Jennings, Z. G., Pastorello, N., Pota, V., Usher, C., Blom, C., Kader, J., Roediger, J. C., Spitler, L. R., Villaume, A., Arnold, J. A., Kartha, S. S., and Woodley, K. A. (2014). The SAGES Legacy Unifying Globulars and GalaxieS Survey (SLUGGS): Sample Definition, Methods, and Initial Results. *Astrophysical Journal*, 796:52.

Brodie, J. P. and Strader, J. (2006). Extragalactic Globular Clusters and Galaxy Formation. *Annual Review of Astronomy and Astrophysics*, 44:193–267.

Brodie, J. P., Usher, C., Conroy, C., Strader, J., Arnold, J. A., Forbes, D. A., and Romanowsky, A. J. (2012). The SLUGGS Survey: NGC 3115, A Critical Test Case for Metallicity Bimodality in Globular Cluster Systems. *Astrophysical Journal*, 759:L33.

Cantiello, M., Blakeslee, J. P., Raimondo, G., Chies-Santos, A. L., Jennings, Z. G., Norris, M. A., and Kuntschner, H. (2014). Globular clusters of NGC 3115 in the near-infrared. Demonstrating the correctness of two opposing scenarios. *Astronomy & Astrophysics*, 564:L3.

Caon, N., Capaccioli, M., and D'Onofrio, M. (1993). On the Shape of the Light Profiles of Early Type Galaxies. *Monthy Notices of the Royal Astronomical Society*, 265:1013.

Capaccioli, M. and Caon, N. (1989). Surface photometry of early-type galaxies. In Grosbøl, P. J., Murtagh, F., and Warmels, R. H., editors, *ESO/ST-ECF Data Analysis Workshop*, volume 31 of *European Southern Observatory Conference and Workshop Proceedings*, pages 107–126.

Cappellari, M., Emsellem, E., Krajnović, D., McDermid, R. M., Serra, P., Alatalo, K., Blitz, L., Bois, M., Bournaud, F., Bureau, M., Davies, R. L., Davis, T. A., de Zeeuw, P. T., Khochfar, S., Kuntschner, H., Lablanche, P.-Y., Morganti, R., Naab, T., Oosterloo, T., Sarzi, M., Scott, N., Weijmans, A.-M., and Young, L. M. (2011). The ATLAS^{3D} project - VII. A new look at the morphology of nearby galaxies: the kinematic morphology-density relation. *Monthy Notices of the Royal Astronomical Society*, 416:1680–1696.

Carrasco, E. R., Conselice, C. J., and Trujillo, I. (2010). Gemini K-band NIRI Adaptive Optics Observations of massive galaxies at 1 z 2. *Monthy Notices of the Royal Astronomical Society*, 405:2253–2259.

Chies-Santos, A. L., Cortesi, A., Fantin, D. S. M., Merrifield, M. R., Bamford, S., and Serra, P. (2013). The nature of faint fuzzies from the kinematics of NGC 1023. *Astronomy & Astrophysics*, 559:A67.

Chies-Santos, A. L., Larsen, S. S., Cantiello, M., Strader, J., Kuntschner, H., Wehner, E. M., and Brodie, J. P. (2012). An optical/NIR survey of globular clusters in early-type galaxies. III. On the colour bimodality of globular cluster systems. *Astronomy & Astrophysics*, 539:A54.

Chies-Santos, A. L., Larsen, S. S., Wehner, E. M., Kuntschner, H., Strader, J., and Brodie, J. P. (2011). An optical/NIR survey of globular clusters in early-type galaxies. I. Introduction and data reduction procedures. *Astronomy & Astrophysics*, 525:A19.

Chomiuk, L., Strader, J., and Brodie, J. P. (2008). The Peculiar Globular Cluster System of the s0 Galaxy NGC 7457. *Astronomical Journal*, 136:234–249.

Coccato, L., Gerhard, O., Arnaboldi, M., Das, P., Douglas, N. G., Kuijken, K., Merrifield, M. R., Napolitano, N. R., Noordermeer, E., Romanowsky, A. J., Capaccioli, M., Cortesi, A.,

De Lorenzi, F., and Freeman, K. C. (2009). Kinematic properties of early-type galaxy haloes using planetary nebulae*. *Monthy Notices of the Royal Astronomical Society*, 394:1249–1283.

Combes, F. and Sanders, R. H. (1981). Formation and properties of persisting stellar bars. *Astronomy & Astrophysics*, 96:164–173.

Conselice, C. J. (2014). The Evolution of Galaxy Structure Over Cosmic Time. *Annual Review of Astronomy and Astrophysics*, 52:291–337.

Cortesi, A., Arnaboldi, M., Coccato, L., Merrifield, M. R., Gerhard, O., Bamford, S., Romanowsky, A. J., Napolitano, N. R., Douglas, N. G., Kuijken, K., Capaccioli, M., Freeman, K. C., Chies-Santos, A. L., and Pota, V. (2013a). The Planetary Nebula Spectrograph survey of S0 galaxy kinematics. Data and overview. *Astronomy & Astrophysics*, 549:A115.

Cortesi, A., Chies-Santos, A. L., Pota, V., Foster, C., Coccato, L., Mendes de Oliveira, C., Forbes, D. A., Merrifield, M. M., Bamford, S. P., Romanowsky, A. J., Brodie, J. P., Kartha, S. S., Alabi, A. B., Proctor, R. N., and Almeida, A. (2016). The SLUGGS survey: chromodynamical modelling of the lenticular galaxy NGC 1023. *Monthy Notices of the Royal Astronomical Society*, 456:2611–2621.

Cortesi, A., Merrifield, M. R., Arnaboldi, M., Gerhard, O., Martinez-Valpuesta, I., Saha, K., Coccato, L., Bamford, S., Napolitano, N. R., Das, P., Douglas, N. G., Romanowsky, A. J., Kuijken, K., Capaccioli, M., and Freeman, K. C. (2011). Unravelling the origins of S0 galaxies using maximum likelihood analysis of planetary nebulae kinematics. *Monthy Notices of the Royal Astronomical Society*, 414:642–651.

Cortesi, A., Merrifield, M. R., Coccato, L., Arnaboldi, M., Gerhard, O., Bamford, S., Napolitano, N. R., Romanowsky, A. J., Douglas, N. G., Kuijken, K., Capaccioli, M., Freeman, K. C., Saha, K., and Chies-Santos, A. L. (2013b). Planetary Nebula Spectrograph survey of S0 galaxy kinematics - II. Clues to the origins of S0 galaxies. *Monthy Notices of the Royal Astronomical Society*, 432:1010–1020.

de Vaucouleurs, G. (1953). The Distribution of Light in Galaxies. *Leaflet of the Astronomical Society of the Pacific*, 6:362.

de Vaucouleurs, G., de Vaucouleurs, A., Corwin, Jr., H. G., Buta, R. J., Paturel, G., and Fouqué, P. (1991). *Third Reference Catalogue of Bright Galaxies. Volume I: Explanations and references. Volume II: Data for galaxies between 0^h and 12^h. Volume III: Data for galaxies between 12^h and 24^h.*

Debattista, V. P., Corsini, E. M., and Aguerri, J. A. L. (2002). A fast bar in the post-interaction galaxy NGC 1023. *Monthy Notices of the Royal Astronomical Society*, 332:65–77.

Douglas, N. G., Arnaboldi, M., Freeman, K. C., Kuijken, K., Merrifield, M. R., Romanowsky, A. J., Taylor, K., Capaccioli, M., Axelrod, T., Gilmozzi, R., Hart, J., Bloxham, G., and Jones, D. (2002). The Planetary Nebula Spectrograph: The Green Light for Galaxy Kinematics. *Publications of the Astronomical Society of the Pacific*, 114:1234–1251.

Doyle, M. T., Drinkwater, M. J., Rohde, D. J., Pimbblet, K. A., Read, M., Meyer, M. J., Zwaan, M. A., Ryan-Weber, E., Stevens, J., Koribalski, B. S., Webster, R. L., Staveley-Smith, L., Barnes, D. G., Howlett, M., Kilborn, V. A., Waugh, M., Pierce, M. J., Bhathal, R., de Blok, W. J. G., Disney, M. J., Ekers, R. D., Freeman, K. C., Garcia, D. A., Gibson, B. K., Harnett, J., Henning, P. A., Jerjen, H., Kesteven, M. J., Knezek, P. M., Mader, S., Marquarding, M., Minchin, R. F., O'Brien, J., Oosterloo, T., Price, R. M., Putman, M. E., Ryder, S. D., Sadler, E. M., Stewart, I. M., Stootman, F., and Wright, A. E. (2005). The HIPASS catalogue - III. Optical counterparts and isolated dark galaxies. *Monthy Notices of the Royal Astronomical Society*, 361:34–44.

Dressler, A. (1980). Galaxy morphology in rich clusters - Implications for the formation and evolution of galaxies. *Astrophysical Journal*, 236:351–365.

Dressler, A., Bigelow, B., Hare, T., Sutin, B., Thompson, I., Burley, G., Epps, H., Oemler, Jr., A., Bagish, A., Birk, C., Clardy, K., Gunnels, S., Kelson, D., Shectman, S., and Osip, D. (2011). IMACS: The Inamori-Magellan Areal Camera and Spectrograph on Magellan-Baade. *Publications of the Astronomical Society of the Pacific*, 123:288.

Dressler, A., Oemler, Jr., A., Couch, W. J., Smail, I., Ellis, R. S., Barger, A., Butcher, H., Poggianti, B. M., and Sharples, R. M. (1997). Evolution since z = 0.5 of the Morphology-Density Relation for Clusters of Galaxies. *Astrophysical Journal*, 490:577–591.

Dressler, A. and Sandage, A. (1983). Rotational velocities and central velocity dispersions for a sample of S0 galaxies. *Astrophysical Journal*, 265:664–680.

Eggen, O. J., Lynden-Bell, D., and Sandage, A. R. (1962). Evidence from the motions of old stars that the Galaxy collapsed. *Astrophysical Journal*, 136:748.

Emsellem, E., Cappellari, M., Krajnović, D., Alatalo, K., Blitz, L., Bois, M., Bournaud, F., Bureau, M., Davies, R. L., Davis, T. A., de Zeeuw, P. T., Khochfar, S., Kuntschner, H., Lablanche, P.-Y., McDermid, R. M., Morganti, R., Naab, T., Oosterloo, T., Sarzi, M., Scott, N., Serra, P., van de Ven, G., Weijmans, A.-M., and Young, L. M. (2011). The ATLAS^{3D} project - III. A census of the stellar angular momentum within the effective radius of early-type galaxies: unveiling the distribution of fast and slow rotators. *Monthy Notices of the Royal Astronomical Society*, 414:888–912.

Faber, S. M., Phillips, A. C., Kibrick, R. I., Alcott, B., Allen, S. L., Burrous, J., Cantrall, T., Clarke, D., Coil, A. L., Cowley, D. J., Davis, M., Deich, W. T. S., Dietsch, K., Gilmore, D. K., Harper, C. A., Hilyard, D. F., Lewis, J. P., McVeigh, M., Newman, J., Osborne, J., Schiavon, R., Stover, R. J., Tucker, D., Wallace, V., Wei, M., Wirth, G., and Wright, C. A. (2003). The DEIMOS spectrograph for the Keck II Telescope: integration and testing. In Iye, M. and Moorwood, A. F. M., editors, *Instrument Design and Performance for Optical/Infrared Ground-based Telescopes*, volume 4841 of Proc. SPIE, pages 1657–1669.

Forbes, D. A., Alabi, A., Brodie, J. P., Romanowsky, A. J., Strader, J., Foster, C., Usher, C., Spitler, L., Bellstedt, S., Pastorello, N., Villaume, A., Wasserman, A., and Pota, V. (2017). The SLUGGS Survey: A Catalog of Over 4000 Globular Cluster Radial Velocities in 27 Nearby Early-type Galaxies. *Astronomical Journal*, 153:114.

Forbes, D. A., Almeida, A., Spitler, L. R., and Pota, V. (2014). Extended star clusters in NGC 1023 from HST/ACS mosaic imaging. *Monthy Notices of the Royal Astronomical Society*, 442:1049–1053.

Forbes, D. A., Brodie, J. P., and Grillmair, C. J. (1997). On the Origin of Globular Clusters in Elliptical and cD Galaxies. *Astronomical Journal*, 113:1652.

Forbes, D. A., Brodie, J. P., and Larsen, S. S. (2001). Bulge Globular Clusters in Spiral Galaxies. *Astrophysical Journal*, 556:L83–L86.

Forbes, D. A., Cortesi, A., Pota, V., Foster, C., Romanowsky, A. J., Merrifield, M. R., Brodie, J. P., Strader, J., Coccato, L., and Napolitano, N. (2012). Radially extended kinematics in the S0 galaxy NGC 2768 from planetary nebulae, globular clusters and starlight. *Monthy Notices of the Royal Astronomical Society*, 426:975–982.

Forte, J. C., Geisler, D., Ostrov, P. G., Piatti, A. E., and Gieren, W. (2001). The Globular Cluster System of the Low-Luminosity Elliptical Galaxy NGC 1427. *Astronomical Journal*, 121:1992–2002.

Fried, J. W. and Illingworth, G. D. (1994). Kinematics of 12 elliptical galaxies. *Astronomical Journal*, 107:992–1002.

Garcia, A. M. (1993). General study of group membership. II - Determination of nearby groups. *Astronomy and Astrophysics, Supplement*, 100:47–90.

Graham, A. W. and Driver, S. P. (2005). A Concise Reference to (Projected) Sérsic $R^{1/n}$ Quantities, Including Concentration, Profile Slopes, Petrosian Indices, and Kron Magnitudes. *Publications of the Astron. Soc. of Australia*, 22:118–127.

Guérou, A., Emsellem, E., Krajnović, D., McDermid, R. M., Contini, T., and Weilbacher, P. M. (2016). Exploring the mass assembly of the early-type disc galaxy NGC 3115 with MUSE. *Astronomy & Astrophysics*, 591:A143.

Gunn, J. E. and Gott, III, J. R. (1972). On the Infall of Matter Into Clusters of Galaxies and Some Effects on Their Evolution. *Astrophysical Journal*, 176:1.

Hargis, J. R., Rhode, K. L., Strader, J., and Brodie, J. P. (2011). The Globular Cluster Population of NGC 7457: Clues to the Evolution of Field S0 Galaxies. *Astrophysical Journal*, 738:113.

Harris, W. E. (2010). Massive star clusters in galaxies. *Philosophical Transactions of the Royal Society of London Series A*, 368:889–906.

Hopkins, P. F., Croton, D., Bundy, K., Khochfar, S., van den Bosch, F., Somerville, R. S., Wetzel, A., Keres, D., Hernquist, L., Stewart, K., Younger, J. D., Genel, S., and Ma, C.-P. (2010). Mergers in ΛCDM: Uncertainties in Theoretical Predictions and Interpretations of the Merger Rate. *Astrophysical Journal*, 724:915–945.

Jedrzejewski, R. I. (1987). CCD surface photometry of elliptical galaxies. I - Observations, reduction and results. *Monthy Notices of the Royal Astronomical Society*, 226:747–768.

Jennings, Z. G., Strader, J., Romanowsky, A. J., Brodie, J. P., Arnold, J. A., Lin, D., Irwin, J. A., Sivakoff, G. R., and Wong, K.-W. (2014). The SLUGGS Survey: HST/ACS Mosaic Imaging of the NGC 3115 Globular Cluster System. *Astronomical Journal*, 148:32.

Kim, D.-W. (1989). Interstellar matter in early-type galaxies - Optical observations. *Astrophysical Journal*, 346:653–674.

Kormendy, J. (1979). A morphological survey of bar, lens, and ring components in galaxies Secular evolution in galaxy structure. *Astrophysical Journal*, 227:714–728.

Larsen, S. S. and Brodie, J. P. (2000). Hubble Space Telescope Observations of Star Clusters in NGC 1023: Evidence for Three Cluster Populations? *Astronomical Journal*, 120:2938–2949.

Larsen, S. S., Brodie, J. P., Huchra, J. P., Forbes, D. A., and Grillmair, C. J. (2001). Properties of Globular Cluster Systems in Nearby Early-Type Galaxies. *Astronomical Journal*, 121:2974–2998.

McCarthy, I. G., Frenk, C. S., Font, A. S., Lacey, C. G., Bower, R. G., Mitchell, N. L., Balogh, M. L., and Theuns, T. (2008). Ram pressure stripping the hot gaseous haloes of galaxies in groups and clusters. *Monthy Notices of the Royal Astronomical Society*, 383:593–605.

McDermid, R. M., Alatalo, K., Blitz, L., Bournaud, F., Bureau, M., Cappellari, M., Crocker, A. F., Davies, R. L., Davis, T. A., de Zeeuw, P. T., Duc, P.-A., Emsellem, E., Khochfar, S., Krajnović, D., Kuntschner, H., Morganti, R., Naab, T., Oosterloo, T., Sarzi, M., Scott, N., Serra, P., Weijmans, A.-M., and Young, L. M. (2015). The ATLAS^{3D} Project - XXX. Star formation histories and stellar population scaling relations of early-type galaxies. *Monthy Notices of the Royal Astronomical Society*, 448:3484–3513.

Miyazaki, S., Komiyama, Y., Sekiguchi, M., Okamura, S., Doi, M., Furusawa, H., Hamabe, M., Imi, K., Kimura, M., Nakata, F., Okada, N., Ouchi, M., Shimasaku, K., Yagi, M., and Yasuda, N. (2002). Subaru Prime Focus Camera – Suprime-Cam. *Publications of the Astronomical Society of Japan*, 54:833–853.

Moody, C. E., Romanowsky, A. J., Cox, T. J., Novak, G. S., and Primack, J. R. (2014). Simulating multiple merger pathways to the central kinematics of early-type galaxies. *Monthy Notices of the Royal Astronomical Society*, 444:1475–1485.

Muratov, A. L. and Gnedin, O. Y. (2010). Modeling the Metallicity Distribution of Globular Clusters. *Astrophysical Journal*, 718:1266–1288.

Napolitano, N. R., Arnaboldi, M., Freeman, K. C., and Capaccioli, M. (2001). Planetary nebulae as mass tracers of their parent galaxies: Biases in the estimate of the kinematical quantities. *Astronomy & Astrophysics*, 377:784–800.

Noordermeer, E., Merrifield, M. R., Coccato, L., Arnaboldi, M., Capaccioli, M., Douglas, N. G., Freeman, K. C., Gerhard, O., Kuijken, K., de Lorenzi, F., Napolitano, N. R., and Romanowsky, A. J. (2008). Testing the nature of S0 galaxies using planetary nebula kinematics in NGC 1023. *Monthy Notices of the Royal Astronomical Society*, 384:943–952.

Norris, M. A., Kannappan, S. J., Forbes, D. A., Romanowsky, A. J., Brodie, J. P., Faifer, F. R., Huxor, A., Maraston, C., Moffett, A. J., Penny, S. J., Pota, V., Smith-Castelli, A., Strader, J., Bradley, D., Eckert, K. D., Fohring, D., McBride, J., Stark, D. V., and Vaduvescu, O. (2014). The AIMSS Project - I. Bridging the star cluster-galaxy divide. *Monthy Notices of the Royal Astronomical Society*, 443:1151–1172.

Norris, M. A., Sharples, R. M., and Kuntschner, H. (2006). GMOS spectroscopy of the S0 galaxy NGC 3115. *Monthy Notices of the Royal Astronomical Society*, 367:815–824.

Oke, J. B., Cohen, J. G., Carr, M., Cromer, J., Dingizian, A., Harris, F. H., Labrecque, S., Lucinio, R., Schaal, W., Epps, H., and Miller, J. (1995). The Keck Low-Resolution Imaging Spectrometer. *Publications of the Astronomical Society of the Pacific*, 107:375.

Oldham, L. J. and Auger, M. W. (2016). Galaxy structure from multiple tracers - I. A census of M87's globular cluster populations. *Monthy Notices of the Royal Astronomical Society*, 455:820–830.

Oser, L., Ostriker, J. P., Naab, T., Johansson, P. H., and Burkert, A. (2010). The Two Phases of Galaxy Formation. *Astrophysical Journal*, 725:2312–2323.

Peacock, M. B., Zepf, S. E., Kundu, A., Maccarone, T. J., Lehmer, B. D., Gonzalez, A. H., and Maraston, C. (2017). Deep Chandra observations of NGC 7457, the X-ray point source populations of a low-mass early-type galaxy. *Monthy Notices of the Royal Astronomical Society*, 466:4021–4028.

Peng, C. Y., Ho, L. C., Impey, C. D., and Rix, H.-W. (2002). Detailed Structural Decomposition of Galaxy Images. *Astronomical Journal*, 124:266–293.

Peng, E., Takamiya, M., Cote, P., West, M. J., Blakeslee, J. P., Ferrarese, L., Jordan, A., and Mei, S. (2006). The Spatial Distributions of Globular Cluster Systems. In *American Astronomical Society Meeting Abstracts*, volume 38 of *Bulletin of the American Astronomical Society*, page 1062.

Pota, V., Forbes, D. A., Romanowsky, A. J., Brodie, J. P., Spitler, L. R., Strader, J., Foster, C., Arnold, J. A., Benson, A., Blom, C., Hargis, J. R., Rhode, K. L., and Usher, C. (2013). The SLUGGS Survey: kinematics for over 2500 globular clusters in 12 early-type galaxies. *Monthy Notices of the Royal Astronomical Society*, 428:389–420.

Quilis, V., Moore, B., and Bower, R. (2000). Gone with the Wind: The Origin of S0 Galaxies in Clusters. *Science*, 288:1617–1620.

Rocha, M., Peter, A. H. G., and Bullock, J. (2012). Infall times for Milky Way satellites from their present-day kinematics. *Monthy Notices of the Royal Astronomical Society*, 425:231–244.

Romanowsky, A. J. and SAGES Team (2013). Multiple Probes of Mass in Early-type Galaxies. In *Probes of Dark Matter on Galaxy Scales*, volume 1.

Saha, A., Armandroff, T., Sawyer, D. G., and Corson, C. (2000). Imaging performance of the mini-mosaic camera at the WIYN telescope. In Iye, M. and Moorwood, A. F., editors, *Optical and IR Telescope Instrumentation and Detectors*, volume 4008 of Proc. SPIE, pages 447–451.

Sandage, A. and Bedke, J. (1994). *The Carnegie Atlas of Galaxies. Volumes I, II.*

Schuberth, Y., Richtler, T., Dirsch, B., Hilker, M., and Larsen, S. (2005). The Outer Cluster System of NGC 1399: Preliminary Results. *ArXiv Astrophysics e-prints.*

Schweizer, F. (2001). Galaxy Interactions: Overview. In *American Astronomical Society Meeting Abstracts #198*, volume 33 of *Bulletin of the American Astronomical Society*, page 830.

Sérsic, J. L. (1963). Influence of the atmospheric and instrumental dispersion on the brightness distribution in a galaxy. *Boletin de la Asociacion Argentina de Astronomia La Plata Argentina*, 6:41.

Shapiro, K. L., Genzel, R., and Förster Schreiber, N. M. (2010). Star-forming galaxies at z ˜ 2 and the formation of the metal-rich globular cluster population. *Monthy Notices of the Royal Astronomical Society*, 403:L36–L40.

Sil'chenko, O. K., Afanasiev, V. L., Chavushyan, V. H., and Valdes, J. R. (2002). Young Stellar Nuclei in Lenticular Galaxies: NGC 5574 and NGC 7457. *Astrophysical Journal*, 577:668–679.

Skrutskie, M. F., Cutri, R. M., Stiening, R., Weinberg, M. D., Schneider, S., Carpenter, J. M., Beichman, C., Capps, R., Chester, T., Elias, J., Huchra, J., Liebert, J., Lonsdale, C., Monet, D. G., Price, S., Seitzer, P., Jarrett, T., Kirkpatrick, J. D., Gizis, J. E., Howard, E., Evans,

T., Fowler, J., Fullmer, L., Hurt, R., Light, R., Kopan, E. L., Marsh, K. A., McCallon, H. L., Tam, R., Van Dyk, S., and Wheelock, S. (2006). The Two Micron All Sky Survey (2MASS). *Astronomical Journal*, 131:1163–1183.

Strader, J., Romanowsky, A. J., Brodie, J. P., Spitler, L. R., Beasley, M. A., Arnold, J. A., Tamura, N., Sharples, R. M., and Arimoto, N. (2011). Wide-field Precision Kinematics of the M87 Globular Cluster System. *Astrophysical Journal, Supplement*, 197:33.

Tully, R. B., Courtois, H. M., Dolphin, A. E., Fisher, J. R., Héraudeau, P., Jacobs, B. A., Karachentsev, I. D., Makarov, D., Makarova, L., Mitronova, S., Rizzi, L., Shaya, E. J., Sorce, J. G., and Wu, P.-F. (2013). Cosmicflows-2: The Data. *Astronomical Journal*, 146:86.

van den Bergh, S. (1976). A new classification system for galaxies. *Astrophysical Journal*, 206:883–887.

van den Bergh, S. (2009). Lenticular Galaxies and their Environments. *Astrophysical Journal*, 702:1502–1506.

Vika, M., Bamford, S. P., Häußler, B., Rojas, A. L., Borch, A., and Nichol, R. C. (2013). MegaMorph - multiwavelength measurement of galaxy structure. Sérsic profile fits to galaxies near and far. *Monthy Notices of the Royal Astronomical Society*, 435:623–649.

Wilman, D. J., Oemler, Jr., A., Mulchaey, J. S., McGee, S. L., Balogh, M. L., and Bower, R. G. (2009). Morphological Composition of z ˜ 0.4 Groups: The Site of S0 Formation. *Astrophysical Journal*, 692:298–308.

Yoon, S.-J., Yi, S. K., and Lee, Y.-W. (2006). Explaining the Color Distributions of Globular Cluster Systems in Elliptical Galaxies. *Science*, 311:1129–1132.

York, D. G., Adelman, J., Anderson, Jr., J. E., Anderson, S. F., Annis, J., Bahcall, N. A., Bakken, J. A., Barkhouser, R., Bastian, S., Berman, E., Boroski, W. N., Bracker, S., Briegel, C., Briggs, J. W., Brinkmann, J., Brunner, R., Burles, S., Carey, L., Carr, M. A., Castander, F. J., Chen, B., Colestock, P. L., Connolly, A. J., Crocker, J. H., Csabai, I., Czarapata, P. C., Davis, J. E., Doi, M., Dombeck, T., Eisenstein, D., Ellman, N., Elms, B. R., Evans,

M. L., Fan, X., Federwitz, G. R., Fiscelli, L., Friedman, S., Frieman, J. A., Fukugita, M., Gillespie, B., Gunn, J. E., Gurbani, V. K., de Haas, E., Haldeman, M., Harris, F. H., Hayes, J., Heckman, T. M., Hennessy, G. S., Hindsley, R. B., Holm, S., Holmgren, D. J., Huang, C.-h., Hull, C., Husby, D., Ichikawa, S.-I., Ichikawa, T., Ivezić, Ž., Kent, S., Kim, R. S. J., Kinney, E., Klaene, M., Kleinman, A. N., Kleinman, S., Knapp, G. R., Korienek, J., Kron, R. G., Kunszt, P. Z., Lamb, D. Q., Lee, B., Leger, R. F., Limmongkol, S., Lindenmeyer, C., Long, D. C., Loomis, C., Loveday, J., Lucinio, R., Lupton, R. H., MacKinnon, B., Mannery, E. J., Mantsch, P. M., Margon, B., McGehee, P., McKay, T. A., Meiksin, A., Merelli, A., Monet, D. G., Munn, J. A., Narayanan, V. K., Nash, T., Neilsen, E., Neswold, R., Newberg, H. J., Nichol, R. C., Nicinski, T., Nonino, M., Okada, N., Okamura, S., Ostriker, J. P., Owen, R., Pauls, A. G., Peoples, J., Peterson, R. L., Petravick, D., Pier, J. R., Pope, A., Pordes, R., Prosapio, A., Rechenmacher, R., Quinn, T. R., Richards, G. T., Richmond, M. W., Rivetta, C. H., Rockosi, C. M., Ruthmansdorfer, K., Sandford, D., Schlegel, D. J., Schneider, D. P., Sekiguchi, M., Sergey, G., Shimasaku, K., Siegmund, W. A., Smee, S., Smith, J. A., Snedden, S., Stone, R., Stoughton, C., Strauss, M. A., Stubbs, C., SubbaRao, M., Szalay, A. S., Szapudi, I., Szokoly, G. P., Thakar, A. R., Tremonti, C., Tucker, D. L., Uomoto, A., Vanden Berk, D., Vogeley, M. S., Waddell, P., Wang, S.-i., Watanabe, M., Weinberg, D. H., Yanny, B., Yasuda, N., and SDSS Collaboration (2000). The Sloan Digital Sky Survey: Technical Summary. *Astronomical Journal*, 120:1579–1587.